



Feature article

Metal complex oligomer and polymer wires on electrodes: Tactical constructions and versatile functionalities



Hiroaki Maeda, Ryota Sakamoto, Hiroshi Nishihara*

Department of Chemistry, Graduate School of Science, The University of Tokyo, 7-3-1 Hongo, Bunkyo-ku, Tokyo 113-0033, Japan

ARTICLE INFO

Article history:

Received 27 February 2013

Received in revised form

5 April 2013

Accepted 8 April 2013

Available online 18 April 2013

Keywords:

Molecular wire

Electron transfer

Modified electrode

ABSTRACT

This review covers recent progress in the construction of metal complex wires on various substrates via the stepwise coordination method, their functions, and the electrochemical evaluation of bis(terpyridine) metal complex oligomer wires on electrodes. In the layer-by-layer process of metal complex wire construction, various combinations of anchor ligands, metal sources, and bridging ligands have been used. The prepared structures show multiple functions, including photocurrent generation, catalytic activity, insulation properties, and long-range electron transport abilities. The electron transport behavior, and the long-range electron transport abilities from the terminal redox site to the electrode via bis(terpyridine)metal complex wires, were evaluated using potential step chronoamperometry. The remarkable long-range electron transport abilities were evidenced in the small values for the attenuation factor, β . The influence of the building blocks in the metal complex wires on the β value and the electron transfer rate constant was demonstrated.

© 2013 Elsevier Ltd. Open access under [CC BY-NC-ND license](http://creativecommons.org/licenses/by-nc-nd/4.0/).

1. General introduction

In recent decades, the size of semiconductor-based electric devices has shrunk from a few hundred micrometers to a few nanometers, and their performance has improved drastically. These electric devices are manufactured using the top-down method, which is the technique that is most commonly used to construct nano-size structures (an example of a technique that can be used in this process is photolithography). However, there is a belief that the top-down method will reach a limit in the near future, because of the restriction on the patterning resolution that is imposed by the wavelength of light used in the photolithography process, the leak current from the nanometer-scale electric circuits, and the enormous manufacturing costs. In order to resolve these problems, another approach to the fabrication of nano-size structures (i.e., the bottom-up approach) has become attractive. In this method, structures are constructed by assembling nano- or angstrom-size elements; for example, molecules, atoms, ions, and nanoparticles. These elements will automatically assemble to form the desired structures via electric, hydrophilic/hydrophobic, and various intermolecular interactions among them. This phenomenon is called self-assembly. The self-assembly bottom-up technique allows fabricating a large number of nanometer systems easily and

inexpensively. Therefore, many researchers have studied the bottom-up method to create new materials or systems, and to establish techniques to control the self-assembly process. In this review, we will present recent researches related to the structures created on substrates via molecular self-assembly using the stepwise coordination process, and we evaluate their electrochemical properties.

2. Modification of substrate surfaces by self-assembled monolayers

2.1. Introduction

The fabrication of electric devices composed of molecules is one of the ultimate goals of nanotechnology. It is expected that molecular-based electronic devices would have magnetic, photo-physical, and chemical properties derived from the compositional molecules; this is different from known silicon-based electric devices. Many research groups have fabricated and reported the basic components of molecular devices such as switches [1] and diodes [2]. In the construction of molecular electric systems, the signal detection from molecules is important to input or output information. In addition, high stability is required in the long-term performance and the responsivity to signals. The immobilization of molecules on electrodes is one of the methods that can be used to fulfill these requirements. Molecules immobilized on electrode surfaces should show more rapid responses and higher durability

* Corresponding author.

E-mail address: nishihara@chem.s.u-tokyo.ac.jp (H. Nishihara).

than molecules in solution. Thus, surface modification with molecules is an important process for the achievement of molecular-based devices.

Langmuir–Blodgett (LB) films [3–5], electropolymerization [6,7], chemical vapor deposition (CVD) [8–10], and self-assembled monolayers (SAMs) are the most commonly used surface modification techniques; the preparation of SAMs on various substrates (such as metal, semiconductor, or metal oxide material surfaces) can be achieved easily via immersion in a solution.

2.2. Fabrication of self-assembled monolayers on substrates

Typical combinations of substrates and molecules are listed in Table 1. The SAM fabrication has been performed on various substrates. Among these, gold, indium tin oxide (ITO), and silicon are most usually used as the platforms for SAMs. Gold is the metal that is most commonly applied as electrodes. Gold has excellent thermal and electric conductivity, and a surface that is inert against heat, humidity, oxidation, and a number of chemical reactions. Gold-coated electrodes are typically prepared using vapor deposition on a silicon or mica substrate, followed by annealing with a hydrogen flame to form an Au(111) surface before use. The treated Au electrode is then immersed in a solution of compounds containing thiol, disulfide, SCN, or SAc moieties to fabricate a SAM [11–25]. The formation process, arrangement, electrochemical properties and conductivity of SAMs on Au electrodes have been investigated previously.

The ITO is a transparent electrode material, and is attractive for electrodes in dye-sensitized solar cells and organic electric luminescence devices. For the modification of ITO surfaces, usually phosphoric acid, trialkoxysilane, and carboxylic acid [28–34] are used. Many studies have reported the photochemical properties of SAMs on ITO surfaces, because the transparency of ITO is suitable for photo-irradiation experiments. Matsuo et al. modified ITO with a mixed SAM containing a C₆₀ fullerene and an iron atom-doped C₇₀ fullerene, and demonstrated that this modified electrode generated a bidirectional photocurrent under irradiation with 340 nm and 490 nm light [31]. Nesterov and coworkers prepared thiophene

SAMs on ITO, and performed additional modifications using electrochemical polymerization [32]. The photocurrent generation in ITO modified with SAMs and poly(3,4-ethylenedioxythiophene) was evaluated in the presence of methyl viologen as an electron carrier, and its photovoltaic performance was superior to that of a control device prepared using the spin-coating method. Our laboratory has also reported photochemically functional SAMs on ITO (Fig. 1) [33]. We modified ITO with 3-ferrocenyl-4'-carboxylazobenzene, and succeeded in the *cis*- and *trans*- isomerization of the azobenzene unit with a single wavelength (546 nm), and in the control of the ferrocene valence state. In another study, we sequentially prepared porphyrin-terminated M(tpy)₂ (tpy = 2,2':6',2''-terpyridine, M = Fe²⁺, Co²⁺, Zn²⁺) wires on an ITO surface modified with 4-[(2,2':6',2''-terpyridin)-4''-yl]benzoic acid [34]. The photo-electron conversion abilities of these wires were evaluated in an Na₂SO₄ aqueous solution containing triethanolamine, and the Co(tpy)₂-bridged system showed the highest quantum efficiency.

Silicon is the most widely used semiconductor and core material in the electronics field. The SAMs on SiO₂ and hydrogen-terminated Si have been reported. Trialkoxysilane or trichlorosilane moieties are used for the modification of SiO₂ surfaces, and SAMs are prepared using the thermal method or the vapor phase method [35–39]. The thermal stability of an organic silane SAM has been investigated, and the SAM was not destroyed at 300 °C under vacuum conditions [39]. Hydrogen-terminated silicon is an attractive substrate, due in part to the fact that Si–C bonds can be formed between the substrate and the immobilized molecules without any SiO₂ insulating layer [40–43,45–50]. The connection of SAMs to a silicon surface via covalent bonds allows making a direct evaluation of the electric properties, and this process also results in high thermal and chemical durability. The hydrosilylation reaction between Si–H bonds and alkyne or alkene molecules is one of the most popular methods for the modification of hydrogen-terminated silicon surfaces. This reaction is typically performed under heated conditions or UV light irradiation, but reactions under mild conditions [48] and under visible light irradiation [49] have also been reported. Recently, Huck and Buriak reported that aromatic electron acceptors (e.g., chlorobenzene) accelerated the UV-

Table 1
Combinations of molecules and substrates for the formation of SAMs.

Substrate	Molecule	Ref.	Substrate	Molecule	Ref.	
Au	R–SH	[11–25]	X–Si (X = Cl, Br, I)	R–OH	[51–55]	
	R–S–S–R			R–MgBr		
	R–SCN			R–Na		
	R–SAc					
Pt	R–SH	[26,27]	GeO ₂	R–SiX ₃ (X = Cl, OMe, OEt)	[61]	
	R–NC		X–Ge (X = Cl, Br)	R–MgBr	[62–66]	
ITO	R–SiX ₃ (X = Cl, OMe, OEt)	[28–34]	H–Ge	R–SH	[67–69]	
	R–PO(OH) ₂			Alkenes		
	R–COOH		H–C	R–SH		
SiO ₂ , glass	R–SiX ₃ (X = Cl, OMe, OEt)	[35–39]	X–C (X = Cl, Br)	Alkenes	[70–74]	
				R–I		
H–Si	Alkynes Alkenes R–OH R–CHO R–SH R–MgBr R–Li	[40–50]	Glassy Carbon	R–N=N–R	[75–77]	
			GaAs	R–MgBr		
			InP	R–SH		
			TiO ₂	R–SNa		
				Alkenes		
				R–I		[78,79]
				R–SH		[80–83]
				R–SH		[84–86]
				Alkenes		[87–89]
				R–CO ₂ H		
	R–PO(OH) ₂					
	R–PO(OH) ₂	[90–92,123]				
	R–Si(OEt) ₃					
	Alkenes	[93–96]				
	R–Si(OMe) ₃					

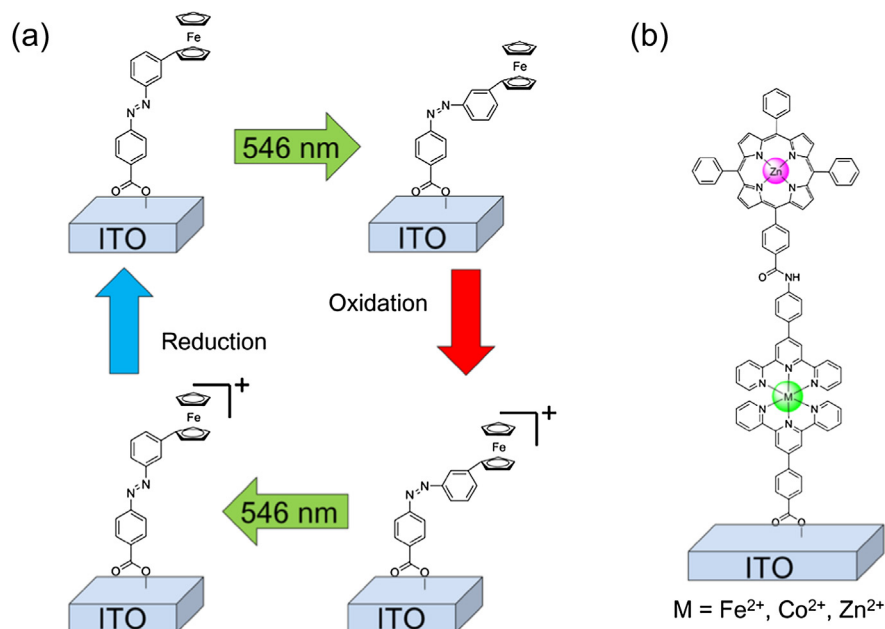


Fig. 1. Photoisomerization of a ferrocene-azobenzene system using single-wavelength light on an ITO electrode. Ref. [33] – Reproduced by permission of The Royal Society of Chemistry. (b) Photocurrent generation system on an ITO electrode. Ref. [34] – Reproduced by permission of The Chemical Society of Japan.

initiated hydrosilylation reaction on H–Si(111) by up to 200 times comparing with the reaction in neat hexadecane [50]. The halogen-termination of silicon is also used to modify silicon substrates. In order to obtain a halogen-terminated silicon surface, hydrogen-terminated silicon is exposed to a halogen source such as PCl_5 , Cl_2 , Br_2 or I_2 [51–55]. In many cases, these halogen-terminated surfaces must be handled under inert conditions, because they have very high reactivity; in contrast, hydrogen-terminated silicon surfaces can exist in air for longer periods. The photoresponse of the redox properties is unique to redox-active SAMs on silicon substrates. This behavior has mainly been investigated in SAMs containing ferrocene moieties. Under dark conditions, the redox reaction of ferrocene is typically irreversible; under irradiation with light, or in a bright place, a reversible redox wave appears. This photo-responsivity derives from the band structure of the semiconductor, and usually redox-active SAMs on n-type silicon exhibit this phenomenon [56–60]. Metals (e.g., Pt) [26,27], carbon substrates [70–79], oxide materials (TiO_2 , Al_2O_3) [87–92,123], and semiconductors (Ge, SiC, GaAs, InP) [61–67,81–86,93–96] have also been employed as substrates for the preparation of SAMs.

There are many possible combinations of substrates and molecules for the formation of SAMs. However, aryl diazonium salt is one of the important compounds for the modification of substrate surfaces. It can be used to fabricate an organic layer with functional groups on various substrates, including carbon, metals, semiconductors, polymers, and insulators [97–99]. The surface modification is achieved using the electrografting method [100–102]. The substrate is used as a working electrode, and is dipped into a solution containing a diazonium salt and a supporting electrolyte. When the potential is swept in the negative direction, the reduction reaction of a diazonium salt occurs on the substrate surface, and the bond between a substrate and an aryl group is formed. The Ar-NH_2 compounds can also be used instead of a diazonium salt [103–107]. In this case, a solution containing an Ar-NH_2 compound, NaNO_2 , and a supporting electrolyte is used. A diazonium salt compound is generated *in situ*, and the surface is modified with an aryl moiety. Recently, other methods that do not require the application of a potential have been reported [108,109]. However, in most cases, the surface modification with a diazonium salt provides an organic

multilayer because of the radical polymerization reaction on the surface [110–113].

3. Fabrication of metal complex oligomer and polymer wires

3.1. Introduction

Many reports on SAMs have stayed within the field of monolayer systems. In general, molecules with a simple structure cannot display multiple functions. If we try to fabricate a multifunctional molecule, its structure will become complicated, and the synthesis method will become cumbersome. Stepwise multilayer fabrication methods have been developed to allow the fabrication of higher-level molecular structures using easy processes. In these methods, SAMs or polymers on a substrate are used as a template for molecular multilayers. Even if each molecular component has a limited function, it is expected that the molecular components that are tandem-arranged using the multilayer construction techniques will provide higher-level functions. Multilayer molecular systems have therefore been the subject of intense research interest, and various multilayer fabrication methods have been reported. These methods use chemical reactions and interactions between molecules; for example, π -stacking, electrostatic interactions, and hydrogen bonds. Using these multilayer fabrication techniques, we can construct molecular structures that have the desired length and array of molecular components.

Usually click chemistry and bond formation reactions using NH_2 groups are used for multilayer fabrication via organic synthesis methods. One example of click chemistry is the copper-catalyzed azide-alkyne Huisgen cycloaddition reaction. Dinolfo and coworkers used 5,10,15,20-tetra(4-ethynylphenyl)porphyrin zinc(II) as an alkyne source, and either 1,3,5-tris(azidomethyl)benzene or 4,4'-diazido-2,2'-stilbenedisulfonic acid disodium salt as an azide source, and fabricated structures with up to 19 layers [114]. The linear growth process was observed using UV-Vis spectroscopy, X-ray reflectivity, ellipsometry, and AFM. Frisbie and coworkers used the imine formation reaction between $-\text{NH}_2$ and $-\text{CHO}$ for the preparation of desired-length π -conjugated molecular wires on Au electrodes (Fig. 2) [115]. The current-voltage (I - V) curves for these

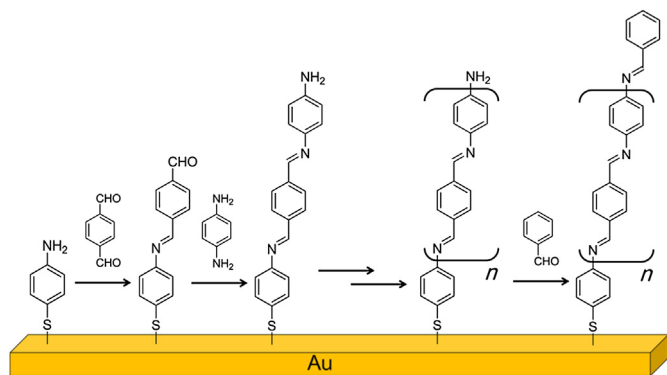


Fig. 2. Stepwise fabrication of a π -conjugated molecular wire, using the organic synthesis method on an Au electrode.

samples were measured using conductive AFM, and their electrical resistances were evaluated. The series of results revealed that the electron transport mechanism was changed by variations in the length of the molecular wire. The resistance of a short molecular wire increased greatly, while that of a long molecular wire showed only a small dependence on the wire length. The electrostatic interaction method uses the ionic interaction between a positively charged compound and a negatively charged compound. Antunes et al. prepared multilayers containing chitosan as a polycation and poly(γ -glutamic acid) as a polyanion, up to six layers, via the sequential dipping of the substrate into solutions [116]. The film-growing process was observed using ellipsometry, QCM, IR spectroscopy, AFM, and zeta potential measurements. The zeta potential measurement after the addition of each layer showed that charge reversal had occurred, and this behavior confirmed the charge interaction between the polyions involved in the multilayer formation. Electropolymerization on a SAM-modified surface can also produce a multilayer structure. Chauvin and coworkers prepared $[M(\text{tpySH})_2]^{2+}$ ($M = \text{Fe}, \text{Ru}$; $\text{tpySH} = 4'-(2-(p\text{-phenoxy})\text{ethane-1-thiol})-2,2':6',2''\text{-terpyridine}$) SAMs on a gold electrode, and fabricated a multilayer using the electrochemical oxidation of thiols [117]. The modified electrode was evaluated using cyclic voltammetry and AFM. Cao and coworkers fabricated calixarene multilayer films connected by hydrogen bonds between protonated amino groups and hydroxyl groups [118]. The fabrication was confirmed using UV–Vis and FT-IR spectroscopy, and the hydrogen bond formation was confirmed by the lower peak shift of N–H stretching vibration. In addition, the stability of this system against metal coordination was revealed by the fabrication of calixarene/ Cu^{2+} multilayer films, while the high-pH environment damaged the multilayer because of the dissociation of hydrogen bonds by OH^- ions.

The stepwise coordination method is one of the most attractive multilayer fabrication methods. One of the benefits of this method is the ability to introduce various metal ions and functional ligands within a molecular wire. It is possible to add not only the functions of ligand molecules, but also the electric, magnetic, and chemical properties of metal complexes to molecular multilayer systems. In this section, we focus on the synthesis and properties of metal complex oligomer and polymer wires constructed using the stepwise coordination method.

3.2. Linear metal complex wires

3.2.1. Fabrication of linear metal complex wires using metal salts

The fundamental process in the stepwise coordination method involves sequential immersion into solutions of a metal ion and a bridging ligand (Fig. 3). First, a substrate is immersed in a solution of

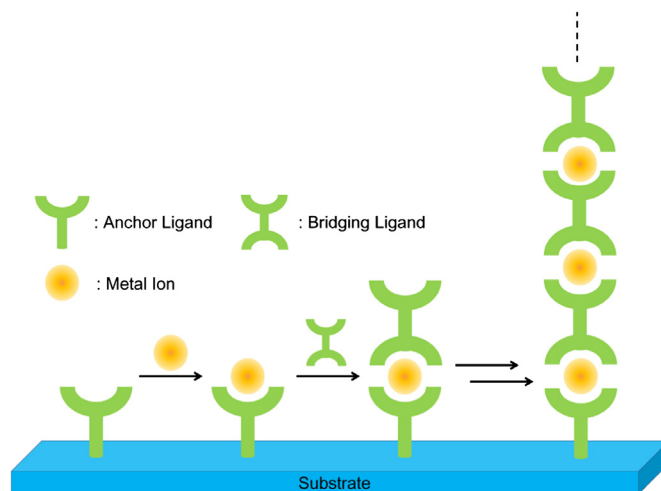


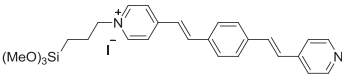
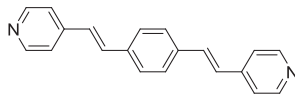
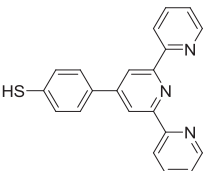
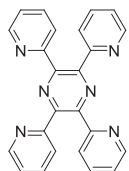
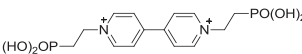
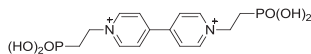
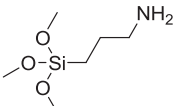
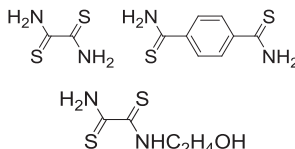
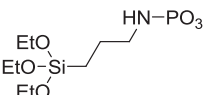
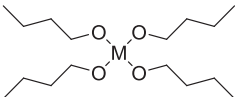
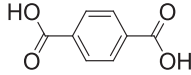
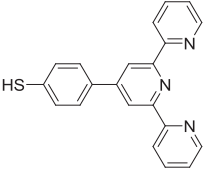
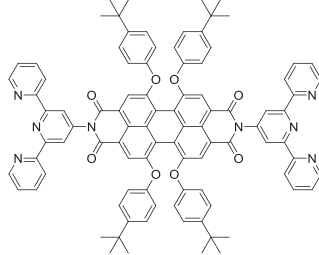
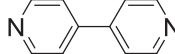
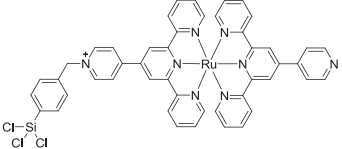
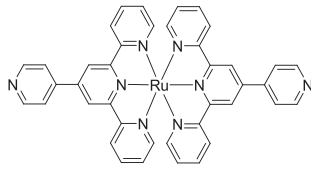
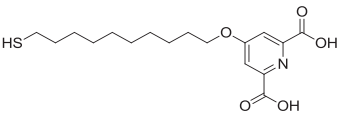
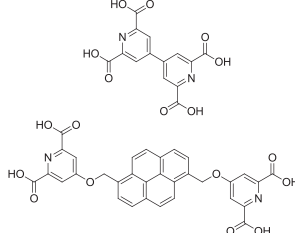
Fig. 3. Multilayer fabrication using the stepwise coordination method.

an anchor ligand that functions as the platform for the multilayers. Next, the modified substrate is dipped into a solution containing a metal ion. Typically, inorganic metal salts are chosen as the metal source. Subsequently, the metal-ion-terminated substrate is immersed in a solution of a bridging ligand, which has a number of coordination sites. In this way, a one-layer metal complex wire is prepared. To lengthen the metal complex wire, these last two processes (immersion in a metal ion solution and a bridging ligand solution) are repeated. A huge variety of metal complex oligomer and polymer wires have been reported; these wires were prepared using a number of combinations of metal ions and ligands, including Pd(II)/pyridine , M(II) or $\text{M(III)/2,2':6',2''\text{-terpyridine}}$, $\text{Cu(II)/carboxylate}$, M(IV)/carboxylate , and other systems (Table 2).

Kosbar et al. reported the stepwise fabrication of multilayers with a number of metal ions on gold substrates modified by 4-mercaptophenyl-2,2':6',2''-terpyridine monolayers [120]. After the formation of a monolayer, the modified film was sequentially immersed in a metal halide solution and a solution of the bridging ligand, tetra-2-pyridinylpyrazine. The constructed metal complex wires were evaluated using UV absorbance spectroscopy, ellipsometry, AFM, and cross-sectional SEM. Among these methods, UV absorbance spectroscopy is most usually used for the evaluation of layer-by-layer growth. The UV absorbance of metal complex wires constructed using Zr(IV) , Ir(III) , and Ru(III) showed a linear increase with the number of coordination cycles. In their discussion, the authors focused on the layer-by-layer construction of Ru(III) metal complex wires. The film thickness values estimated from ellipsometry and AFM measurements increased linearly with the number of coordination steps. This series of results suggested the metal complex wires were fabricated quantitatively. The ionic radius of the metal ion was important in growing molecular wires with at least five layers. Metal ions with effective ionic radii from 66 pm to 73 pm were suitable for the multilayer formation. However, it was difficult to construct multilayers using some metal ions with smaller ionic radii. In most cases of metal ions with radii larger than 73 pm, no stepwise fabrication was observed.

Sugimura et al. fabricated multilayer wires anchored by M(OBu)_4 ($M = \text{Zr(IV)}, \text{Ti(IV)}$) on an Si substrate [124]. The M(OBu)_4 was used as an anchor moiety and coordination metal source. An oxidized Si(100) or Si(111) substrate was immersed in a M(OBu)_4 solution, and the modified substrate was then dipped in a solution of terephthalic acid (TPA). These two processes were repeated to construct multiple layers. The fabricated multilayers were characterized using XPS, grazing incidence X-ray reflectivity

Table 2
Combinations of substrates, metal ions and ligands for the formation of multilayers using the stepwise coordination method.

Substrate	Anchor ligand	Metal ion	Bridging ligand	Ref.
Glass, ITO, Si		Pd ²⁺		[119]
Au		Ti ⁴⁺ , Ir ⁴⁺ , Pt ⁴⁺ , W ⁴⁺ , Rh ³⁺ , Ti ³⁺ , Ir ³⁺ , Ru ³⁺ , Sn ⁴⁺ , Zr ⁴⁺ , Cu ²⁺		[120]
Glassy carbon		Zr ⁴⁺		[121]
Sapphire (0001), glass		Cu ²⁺		[122]
Aluminium alloy, Si		Zr ⁴⁺	(OH) ₂ PO(CH ₂) ₁₂ PO(OH) ₂	[123]
SiO ₂	 M = Zr, Ti	Zr ⁴⁺ , Ti ⁴⁺		[124]
Au		Fe ²⁺		[125]
Quartz, Si	Poly(ethylenamine)	Pd ²⁺		[126]
Glass, Si		Ag ⁺ , Cu ²⁺		[127]
Au		Cu ²⁺ , Fe ³⁺ , Co ²⁺		[128]

(continued on next page)

Table 2 (continued)

Substrate	Anchor ligand	Metal ion	Bridging ligand	Ref.
ITO		Cu^{2+}		[129]
Quartz, ITO, Si		Ru^{3+}		[130]
Au		Cu^{2+} , Zr^{4+}	 $\text{HS}(\text{CH}_2)_4\text{PO}(\text{OH})_2$ 	[131]
Au		Zn^{2+}		[132]
Au		Zr^{4+} , Hf^{4+}		[133]
Quartz, mica		Pd^{2+}		[134]
Au		Zr^{4+}		[135]

(GIXR), and AFM. The six-layer Zr/TPA sample showed a peak derived from Zr 3d in the XPS measurements. In the C1s region, two peaks appeared at approximately 286 eV and 290 eV. The lower energy peak corresponded mainly to the aromatic carbon atoms of TPA, and the higher-energy peak originated from the coordination of carboxyl groups to Zr(IV) ions. When the XPS spectrum of one TPA monolayer sandwiched between two Ti(IV) ions was measured, Ti 2p and C 1s peaks were observed. The C 1s peaks shifted to a lower energy, because the peak at approximately 285 eV corresponded to the carbons in TPA and the alkyl chains of the butoxide groups on the surface. The peak at approximately 289 eV also corresponded to two types of C–O bonds; specifically, the coordination of the butoxide groups and carboxyl groups in TPA with Ti(IV) ions. The GIXR measurements were performed on five pairs of M(IV)/TPA layers. The calculated curves agreed well with the experimental results. These results suggested that the five-layer M(IV)/TPA structures were fabricated as expected. However, according to the authors, the degree of agreement was worse for the Ti/TPA sample than for the Zr/TPA sample, because the level of disorder was higher in Ti/TPA than in Zr/TPA. This disordered behavior was further revealed by AFM measurements. The AFM image of the Ti/TPA/Ti sample showed that the step-terrace structure of the substrate was retained; however, it disappeared when two pairs of Ti/TPA layers were fabricated.

Multilayer fabrication with terpyridine-functionalized perylene bisimide chromophore (TPBI) was performed by Tuccitto et al. [125]. Perylene bisimides are very attractive compounds, because they show strong luminescence, light fastness, and n-type semiconductor behavior [136,137]. The Fe/TPBI multilayers were constructed sequentially on a gold electrode that was modified with the mixed SAM of 4'-p-mercaptophenyl-2,2':6',2''-terpyridine and mercaptobenzene. The ToF-SIMS spectra of a single-layer sample showed the peaks related to the anchor ligand, while only the peaks of the perylene bisimide iron-based complex were observed in the spectra of a 28-layer sample. This result suggested the growth of multilayers only indirectly, because TOF-SIMS cannot detect the underlying layers. The details of the multilayer fabrication were discussed in terms of UV–Vis spectroscopy and AFM observation results. The UV–Vis absorption peak intensity at 589 nm derived from the perylene bisimide iron complex showed a linear increase with the number of coordination cycles. AFM measurements of multilayers on patterned substrates also confirmed the extension of the multilayers. The step height obtained from a histogram analysis increased linearly with the number of layers. The estimated average thickness of a single layer was approximately 2.7 nm. This value corresponded to the expected value for an approximately perpendicular, standing multilayer. Tuccitto et al. investigated the ultrafast time-resolved spectroscopy to examine the photophysical behavior of the 28-layer system. This measurement revealed that the energy absorbed by the multilayer was transferred to the gold electrode in sub-picosecond processes.

3.2.2. Functions of metal complex wires

As shown in Table 2, various metal complex wires have been constructed, and their formation processes have been evaluated. Their functions have attracted much attention, because of the expectation that multilayer systems will provide more effective and diverse functions than monolayer systems. Recently, the catalytic activity of a palladium–pyridine multilayer system, and the photocurrent generation systems were investigated, and their effective capabilities were reported [126,128,131].

Cao and coworkers reported an approach using the metal ions in metal complex wires as a catalyst by Ref. [126]. The authors coated quartz slides or single crystal silicon slides with poly(ethylenimine) (PEI, MW = 60000), and then prepared metal complex wires using PdCl₂ and 4,4'-bipyridyl (bpy), employing the stepwise

coordination method. The prepared metal complex wires were evaluated using UV–Vis spectroscopy, AFM, and XPS measurements. The extension of the PEI-(PdCl₂/bpy)_n wires was confirmed by the linear increase in the UV absorption at 276 nm with the number of coordination cycles, *n*, and the Pd oxidation state in the PEI-(PdCl₂/bpy)_n multilayers was determined as +2 valence from the XPS measurements. The authors used 10-layer multilayer PEI-(PdCl₂/bpy)₁₀ containing 3.6 μg (3.4 × 10⁻⁶ mol%) of Pd ions as a catalyst for the Heck reaction. The reaction conditions were optimized by investigating the effects of bases and solvents, using bromobenzene and styrene as reagents. The highest yield (94%) was achieved when Na₂CO₃ and DMF were used as the base and solvent, respectively. In addition, the turnover numbers (TONs) for the Heck reaction with the Pd metal complex multilayer catalyst were as high as 2.0 × 10⁷. This reaction was applied to various combinations of reagents, and most of them showed moderate to high yields.

Lambert and McGimpsey's group and Thompson's group reported photocurrent-generating systems. The former group used a pyrene-based bridging ligand and three types of metal ions: Cu(II), Co(II), and Fe(III) [128]. The stepwise fabrication process was observed using contact angle measurements, ellipsometry, grazing incidence IR spectroscopy, cyclic voltammetry, and impedance spectroscopy. These characterization methods revealed the formation of well-ordered SAMs, and the assembly of the films through specific metal–ligand interactions. The photocurrent-generation behaviors of four types of films were measured in the presence of methyl viologen for the cathodic photocurrent measurements, and in the presence of triethanolamine for the anodic photocurrent measurements. All of the films showed the photocurrent-generating behavior; however, the multilayer shown in Fig. 4(a) with a Cu(II) metal center afforded the largest cathodic photocurrent values, while the Fe(III)-metal center multilayer gave the strongest anodic photocurrent values.

Thompson's group prepared a donor–accepter system on an Au electrode (Fig. 4(b)) [131]. The characterization was performed using UV–Vis spectroscopy, ellipsometry, and AFM measurements. The photocurrent generation behaviors of POR₃/PV₃, ZOR₃/PV₃, and ZOR₂POR/PV₃ were measured in a 0.1 M LiClO₄ solution containing 0.025 M viologen, under white light illumination (390–540 nm). The short circuit current densities of the illuminated modified electrode at 0 V vs. SCE were 18 and 21 μAcm⁻², and the calculated quantum yields of POR₃/PV₃ and ZOR₃/PV₃ were 2.4% and 2.3%, respectively. The short-circuit current density and quantum yield of the hetero porphyrin system, ZOR₂POR/PV₃, were 26 μAcm⁻² and 3.5%, respectively. The fill factors and maximum power rectangles of these devices were calculated as 37%, 58%, and 50%, and 4.3, 6.3 and 7.6 μWcm⁻² for POR₃/PV₃, ZOR₃/PV₃, and ZOR₂POR/PV₃, respectively. The higher quantum yield and filling factor for ZOR₂POR/PV₃ were derived from the improvement of the photo-induced charge separation that resulted from the effective array of the redox potentials and the optical energy gaps of the molecules in the wire.

3.3. Fabrication of branched metal complex oligomer and polymer wires

Most reports of multilayer fabrication using the stepwise coordination consider linear wires. Recent reports describe the construction of branched structures using a bridging ligand with three coordination sites. For example, Shekhah et al. used 1,3,5-benzenetricarboxylic acid (BTC) as a bridging ligand, and prepared oriented metal organic polymers on a 16-mercaptohexadecanoic acid SAM in a layer-by-layer fashion [132]. The fabricated structure was characterized using XPS, NEXAFS, IRRAS, and AFM observations of an SAM, laterally patterned surface.

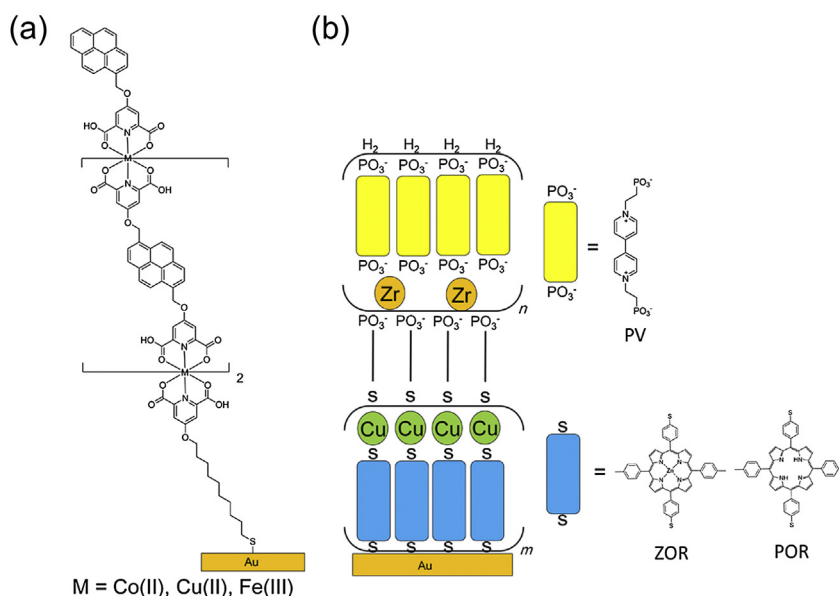


Fig. 4. Photocurrent generation systems. Adapted with permission from Ref. [128]. Copyright (2008) American Chemical Society. Adapted with permission from Ref. [131]. Copyright (2002) American Chemical Society.

The IRRAS spectra of the BTC multilayers on the SAM revealed the stepwise construction; this was confirmed by the linear increase in the peak area for the COO band in IRRAS spectra with increasing number of coordination cycles. The gas-loading properties of four- and eight-layer coordination polymers were researched. The IRRAS spectra demonstrated the reversible exchange between the water in the BTC polymer and NH_3 . The structural model in Fig. 5 was maintained by these exchange experiments.

Rubinstein and coworkers prepared branched structures on a SAM-modified gold electrode using tridentate hexahydroxamate ligands, and $M(\text{IV})$ ions ($M = \text{Zr}, \text{Hf}$) [133]. The stepwise fabrication process was observed using ellipsometry, water contact angle measurements, UV–Vis spectroscopy, and AFM. The film thickness values determined from these measurement techniques showed good agreement with each other, and increased linearly with increasing number of layers. The intermolecular cross-linking of the branched coordination structures was more extensive than that of linear structures, and it increased with the number of coordination layers, thereby improving the mechanical durability. The normal and lateral breakpoint forces, evaluated using AFM, increased with the number of layers, and the branched structures showed much higher

stability than the linear structures. In addition, the electrical properties were evaluated using I – V curve measurements, which were performed using conductive AFM. The data showed that the branched multilayer systems worked as dielectric layers, and the breakdown voltages were 5 MV/cm for the three-layer system and 8 MV/cm for the five-layer system. These values were on the same order as those of ultrathin silicon oxide layers.

3.4. Metal complex wires containing clusters or metal complexes as building blocks

Metal complexes, metal clusters, and metal-coordinated phthalocyanine can also perform as building blocks in the stepwise coordination process (in place of metal salts), because they have coordination sites that can contribute to wire growth (Table 3).

For example, Abe et al. succeeded in the multilayer fabrication of Ru tri-nuclear clusters on gold electrodes [138]. The authors immobilized $[\text{Ru}_3(\mu_3\text{-O})(\mu\text{-CH}_3\text{COO})_6(\text{bpy})_2(\text{CO})]$ (bpy = 4, 4'-bipyridine) clusters SAM on gold electrodes. Next, the CO-terminated SAM was changed to an H_2O -terminated SAM by applying a potential of +0.80 V vs. Ag/AgCl, and the sample was

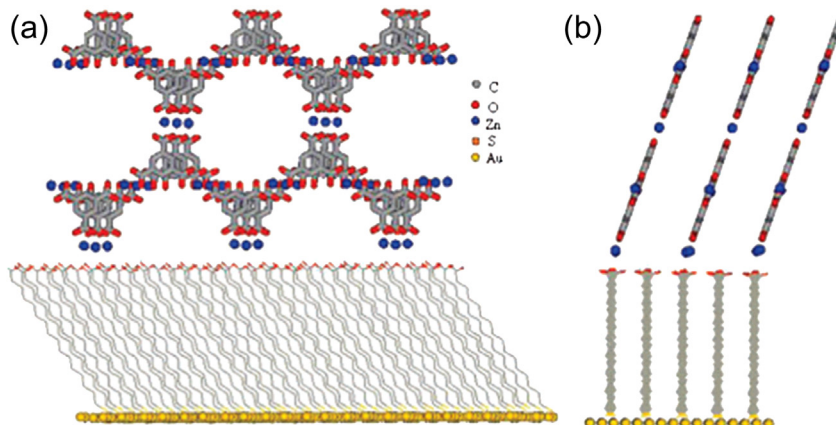


Fig. 5. Proposed model of a stepwise-prepared structure; (a) front view, (b) side view. Reprinted with permission from Ref. [132]. Copyright (2007) American Chemical Society.

Table 3
Combinations of substrates, metal complexes, or metal clusters and ligands for the formation of multilayers using the stepwise coordination method.

Substrate	Anchor ligand	Metal complex, metal cluster	Bridging ligand	Ref.
Au				[138]
Quartz, Si				[139]
Quartz, ITO, Si		$Ru_3(CO)_{12}$		[140]
ITO				[141]
Au				[142]
Au				[143]

then immersed in a solution of Ru_3 clusters. These two processes (i.e., electrolysis for the preparation of CO-free terminal groups, and immersion in a Ru_3 cluster solution) were repeated to fabricate a multilayer structure. The quantitative fabrication of the multilayers was confirmed by the linear increase in the charge derived from the CO-free Ru_3 clusters, and the relative intensity ratio of $I\{\nu_s(COO)\}/I\{\nu(CO)\}$ in the Fourier transform infrared reflection absorption spectra of the CO-terminated Ru_3 clusters.

Stepwise fabrication using a ruthenium-coordinated phthalocyanine was reported by Zhao et al. [141]. After modification of a substrate using the *in situ* diazonium salt-generation method, the pyridine-terminated substrate was immersed in a solution of (phthalocyaninato)ruthenium(II) ($RuPc$), and then dipped into a

solution of pyridine-modified multiwall carbon nanotubes (Py(Ar)-MWCNTs). The prepared multilayer was evaluated using UV–Vis absorption spectroscopy, SEM, and cyclic voltammetry. In the UV–Vis spectra, the peak intensities at 332 nm and 670 nm, which were attributed to the B-band and Q-band of $RuPc$, respectively, increased linearly with the number of layers, suggesting a quantitative layer-by-layer process. In the cyclic voltammograms, the oxidation peak current of $Ru^{3+/2+}$ at 0.78–0.82 V vs. $Ag/AgCl$ increased until a nine-layer structure was achieved; subsequently, however, the peak current started to decay. Photocurrent measurements were also performed on these multilayer systems. The photocurrent increased with the number of layers, and the nine-layer film showed the highest photocurrent density. However,

films with more than nine layers showed low photocurrent densities, due to increases in the internal electrical resistance and/or charge carrier recombination.

Multilayer cluster wires of several nanometers in length were constructed by Lin and Kagan [143], and the films were evaluated using AFM, UV–Vis absorption spectroscopy, and CV. In the cyclic voltammogram of a five-layer film, a redox peak derived from the rhodium clusters was observed, and the peak current was proportional to the scan rate. The linear increase in the peak intensity and the film thickness revealed by the UV–Vis spectra and AFM results confirmed the quantitative extension of the wires. In order to measure the electric properties of these rhodium cluster wires, metal–molecule–metal devices were fabricated. Electrodes with 60–80 nm gaps were prepared using electron-beam lithography, and were connected using the wires. The I – V curve for this device showed voltage-controlled negative differential resistance in the first scan cycle.

4. Electrochemical analysis of bis(terpyridine)metal complex oligomer wires

4.1. Fabrication of bis(terpyridine)metal complex oligomer wires on gold electrodes

The electrochemical properties of stepwise-fabricated metal complex oligomer wires are of great interest, because they have the potential to improve the electron transport in molecular devices or high-level functionalized molecular structures. We researched the layer-by-layer fabrication, the electron transfer behavior, and the long-range electron transport abilities of π -conjugated bis(terpyridine)metal complexes ($M(\text{tpy})_2$). The construction of $M(\text{tpy})_2$ multilayers was achieved via the sequential immersion of an anchor ligand (A^1 – A^3)-modified Au/mica substrate into a metal ion (Fe^{2+} , Co^{2+} or Co^{3+}) solution and a bridging ligand (L^1 – L^7) solution (Fig. 6) [144–151]. In the case of Co^{2+} , the oxidation process of $[\text{Co}(\text{tpy})_2]^{2+}$ was added after the immersion in a bridging ligand solution. When we used L^1 – L^6 , linear-structure wires were fabricated. The $M(\text{tpy})_2$ metal complex wires were evaluated using cyclic voltammetry (CV), STM, and SEM. Fig. 7(a) shows cyclic voltammograms for $A^1(\text{FeL}^2)_n$. A reversible redox couple derived from $[\text{Fe}(\text{tpy})_2]^{3+/2+}$ was observed at approximately 0.6 V vs. Fc^+/Fc , and the intensity increased with the number of coordination cycles, n . In addition, the surface coverage values estimated from the integration of the peak areas increased linearly with the number of layers (Fig. 7(c)). These results suggest that a quantitative complex formation reaction had occurred on the gold substrate. The longest bis(terpyridine)metal complex wire prepared in our laboratory was $A^1(\text{CoL}^1)_{47}$, which had 47 $\text{Co}(\text{tpy})_2$ units. Cross-sectional SEM images of $A^1(\text{CoL}^1)_{47}$ showed a structure with a height of ca. 100 nm. This value agreed with the expected result, because the one-layer thickness was approximately 2 nm.

We could fabricate not only homo metal complex wires but also heterometal complex wires using the stepwise coordination method. The $A^1(\text{CoL}^1)_{10}(\text{FeL}^1)_5$, which had 10 $\text{Co}(\text{tpy})_2$ units connected with 5 $\text{Fe}(\text{tpy})_2$ units, and $A^1\text{CoT}^3$, which was composed of $\text{Co}(\text{tpy})_2$ and cyclometallated Ru complexes, were fabricated and evaluated using CV measurements.

In addition, we could construct bis(terpyridine)metal complex wires with a branched structure using the three-way bridging ligand L^7 . It was expected that the number of metal complexes would be $I_0(2^n - 1)$ when the n th branched wire was prepared, where I_0 is the number of metal complexes in the first layer. Cyclic voltammograms for $A^1(\text{FeL}^7)_n$ are shown in Fig. 7(b), and the estimated number of redox active $\text{Fe}(\text{tpy})_2$ complexes in the branched wires increased as expected until $n = 4$ (Fig. 7(c)). After $n = 5$, the

quantitative growth of the branched wires was not observed, because of the steric hindrance between the branched wires or intrawires, and the contact between the front edge of wire and the electrode surface. These results were supported by the predictions from the molecular model. We believe that the branched wires had a steric structure, different from that of linear wires. We performed STM measurements to observe the topology of the branched wires. When the anchor ligand A^1 was immobilized on gold substrates, the thiol exchange method was used to prepare a low-density packed surface. The prepared branched wire samples, $\text{Au}-A^1\text{FeL}^2(\text{FeL}^7)_n$ ($n = 2$ – 5), showed the oval structures which were sparsely distributed on the surface. The size of these structures were the same as that of the model molecule (Fig. 8). Thus, it was considered that an identical (to that of the model molecule) three-dimensional structure was fabricated on the gold surface.

4.2. Fabrication of bis(terpyridine)iron complex oligomer wires on hydrogen-terminated Si(111)

We constructed the $M(\text{tpy})_2$ metal complex wires not only on gold electrodes, but also on hydrogen-terminated silicon(111) surfaces [152]. We used 4'-ethynyl-2,2':6',2''-terpyridine (A^4) as an anchor ligand (Fig. 9). After the immobilization of A^4 using a hydrosilylation reaction, the modified silicon was immersed alternately in an ethanol solution of Fe^{2+} ions and a chloroform solution of L^2 , to prepare a multilayer structure.

The constructed wires were evaluated using CV, AFM, and XPS. A reversible redox peak was observed in the CV measurements, and the surface coverage values estimated from the oxidation peak were proportional to the number of coordination cycles. The AFM images of three-layer wires revealed a convex structure with a height of 4.5 nm, which corresponded to the estimated value of 4.8 nm. In the XPS spectra, the peak intensity of each element (i.e., Fe 2p, N 1s, and F 1s) increased with the number of coordination cycles. This series of results suggested that the $\text{Fe}(\text{tpy})_2$ complex wires were fabricated quantitatively on the hydrogen-terminated silicon surface. In addition, we found that branched-structure $\text{Fe}(\text{tpy})_2$ wires could also be prepared on H–Si(111) surfaces. One of the important characteristics of semiconductors is the fact that their electric properties can be modulated by changing the doping density and species. Two-layer wires were prepared on low-doped n-type H–Si(111) surfaces, and CV measurements were performed under Xe lamp irradiation, and under dark conditions. A reversible redox peak was observed at approximately 0.6 V under Xe lamp irradiation, while only the cathodic peak appeared under dark conditions. The appearance of the anodic peak under light irradiation and its disappearance under dark conditions could be reversed for up to 50 cycles, illustrating the durable photo-responsivity of the $\text{Fe}(\text{tpy})_2$ redox properties.

Recently, we developed a new method to immobilize arene compounds on H–Si(111) and H–Ge(111) surfaces [153]. A new synthesis method for the formation of Si–aryl or Ge–aryl bonds, catalyzed by Pd(0) or Rh(I) in the presence of a base, was developed previously in our laboratory [154–162]. This reaction could introduce aryl iodides with various substituent groups to the hydrosilane in a one-step reaction, without protecting groups. We recently reported the Pd-catalyzed arylation of tris(trimethylsilyl)silane, whose structure is similar to that of H-terminated silicon, and arylated products were synthesized in good to high yields of up to 89% (Fig. 10(a)) [163]. Thus, we attempted to modify the hydrogen-terminated silicon surfaces with Ar–I compounds using this Pd-catalyzed arylation reaction (Fig. 10(b)). In order to optimize the reaction conditions, 4-iodo-ferrocenylbenzene was chosen as an Ar–I compound; this was because ferrocene shows good reversible redox peaks, which simplified the estimation of the

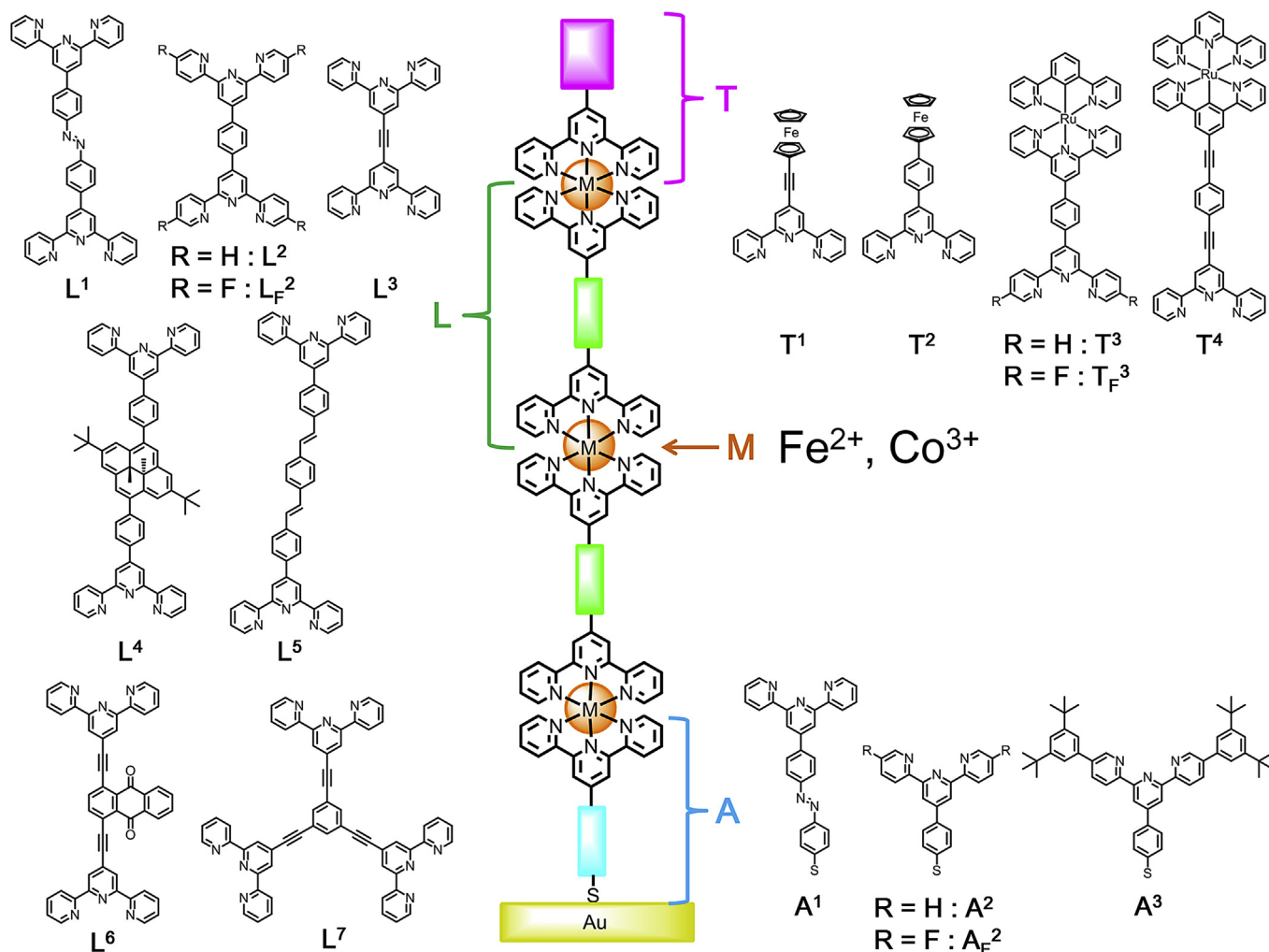


Fig. 6. Building blocks for the multilayer formation of $M(tpy)_2$ metal complex oligomer wires on an Au substrate.

surface coverage. The reaction with 0.8 mM $Pd(Pt-Bu_3)_2$ in 1,4-dioxane at 100 °C for 20 h resulted in the best surface coverage. However, when these reaction conditions were used, palladium nanoparticles were formed. The concentration of the Pd catalyst was therefore decreased to 0.08 mM. The arylation reaction on the H–Si surface was able to proceed at this low concentration of Pd catalyst. We also showed that this reaction could be used to modify

a hydrogen-terminated Ge(111) surface. In order to check the scope for the application of this reaction, we immobilized an H-terminated Si(111) surface using 4-iodo-1H-imidazole or 9-(4-iodophenyl)anthracene, and evaluated the results using XPS and fluorescent spectroscopy. The Si–C bond formation was observed in the photoelectron spectra of the imidazole-modified silicon, and fluorescence at approximately 420 nm appeared in the fluorescent

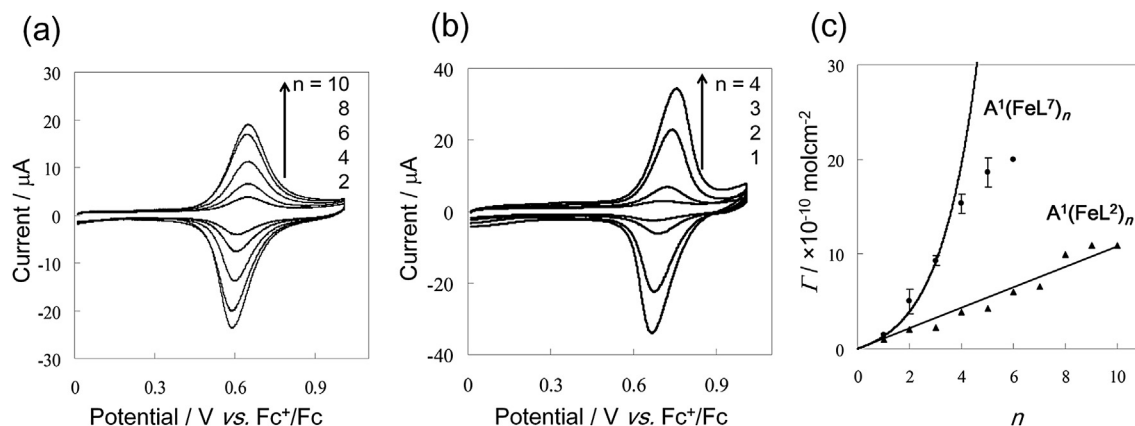


Fig. 7. (a) Cyclic voltammograms of $A^1(FeL^2)_n$, (b) cyclic voltammograms of $A^1(FeL^7)_n$, and (c) relation between the coverage values and the coordination cycle, n . From Ref. [146]. Copyright © 2007 by John Wiley & Sons, Inc. Reprinted by permission of John Wiley & Sons, Inc.

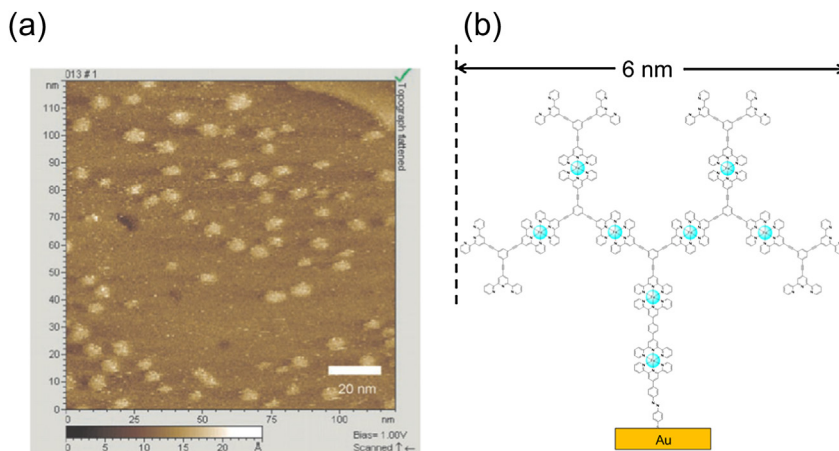


Fig. 8. (a) STM image of $A^1FeL^2(FeL^7)_3$ and (b) the ideal structure of $A^1FeL^2(FeL^7)_3$. From Ref. [146]. Copyright © 2007 by John Wiley & Sons, Inc. Reprinted by permission of John Wiley & Sons, Inc.

spectrum of the anthracene-modified silicon. The $Fe(tpy)_2$ complex wire fabrication was performed using A^5 as an anchor ligand. After the A^5 was immobilized via the Pd-catalyzed arylation, the metal complex wires were elongated in a layer-by-layer process. Cyclic voltammograms of $A^5(FeL^2)_n$ ($n = 2, 4, 6, 8, 10$) showed an increase of the redox peak with increasing n , and the relation between the surface coverage and the number of coordination cycles was proportional. In addition, AFM images of $A^5(FeL^2)_n$ ($n = 2, 4, 10$) showed that the convex structures were sparsely distributed. The estimated heights of these structures were 4.3 nm ($n = 2$), 7.3 nm ($n = 4$), and 17.0 nm ($n = 10$). These values correspond to the expected height; that is, $1.6 \text{ nm} \times n\text{-layers} + 1.1 \text{ nm}$ (the height of A^5). These results suggested that quantitative stepwise fabrication was achieved on the silicon wafer that had been modified by the Pd-catalyzed Si–aryl bond formation reaction.

4.3. Electron transfer properties of bis(terpyridine)iron complex wires on Au

The $M(tpy)_2$ metal complex oligomer wires fabricated using the stepwise coordination method contained regularly ordered redox

active metal complexes. The manner in which an electron moves in this ordered metal complex wire is attractive, because the electron transport behavior in this case is expected to be different from that in randomly oriented metal complex systems. Potential step chronoamperometry (PSCA) is one of the most useful methods to examine the electron movement process. Existing polymers with random array redox-active species show a one-dimensional relationship between the current and time in PSCA measurements. This current–time relation is similar to diffusion behavior, and can be expressed using the Cottrell Equation (1) [164]:

$$i(t) = nFAC(D_{app}/\pi t)^{1/2} \quad (1)$$

where n is the number of electrons involved in the redox reaction, F is the Faraday constant, A is the electrode area, C is the concentration of redox species in the analyte, and D_{app} is the diffusion coefficient. However, the results of PSCA measurements on our $A^1(FeL^2)_n$ and $A^1(FeL^7)_n$ systems did not show a current decay that followed the Cottrell equation; instead, they showed a plateau region in which the current remained almost constant. An analysis of the current–time decay was attempted by hypothesizing the

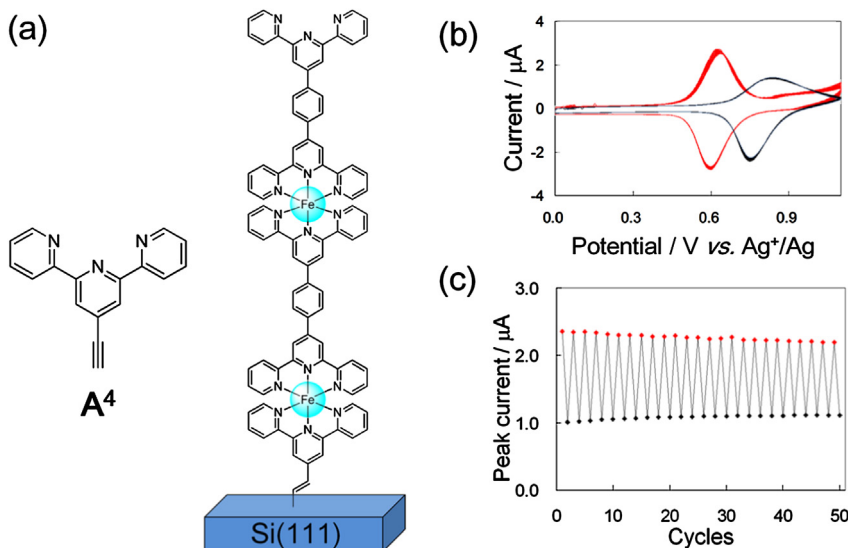


Fig. 9. (a) Structures of A^4 and two-layer wires on a hydrogen-terminated silicon surface, (b) cyclic voltammograms of $A^4(FeL^2)_2$ under Xe lamp irradiation (red line) and under dark conditions (black line), and (c) the anodic peak currents vs. number of potential scan cycles. Ref. [152] – Reproduced by permission of The Royal Society of Chemistry.

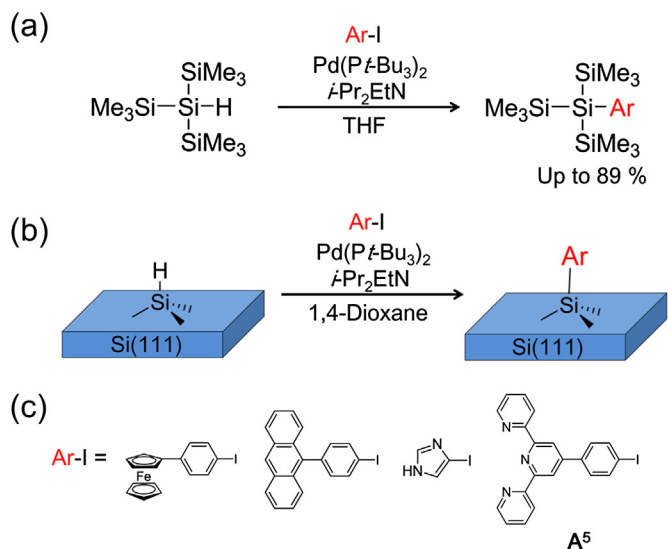


Fig. 10. (a) Arylation reaction of tri(methylsilyl)silane catalyzed by a palladium catalyst. (b) Palladium-catalyzed modification method for an H-terminated Si(111) surface, and (c) the immobilized compounds.

electron transfer mechanism in a single metal complex wire, based on a sequential electron hopping (Fig. 11). The backward electron transfer could be neglected by applying a sufficiently high overpotential to a sample. When the oxidized-form metal complex is reduced to form the metal complex, the electron kinetics in the case of the n th complex in the sequence can be written using the following equations: $d[\text{Ox}_1]/dt = -k_1[\text{Ox}_1] + k_2([\text{Ox}_1]_0 - [\text{Ox}_1])$, $[\text{Ox}_2] \frac{d[\text{Ox}_2]/dt = -k_2([\text{Ox}_1]_0 - [\text{Ox}_1])[\text{Ox}_2] + ([\text{Ox}_3]_0/[\text{Ox}_2]_0)k_2([\text{Ox}_2]_0 - [\text{Ox}_2])[\text{Ox}_3]}{d[\text{Ox}_3]/dt = -([\text{Ox}_3]_0/[\text{Ox}_2]_0)k_2([\text{Ox}_2]_0 - [\text{Ox}_2])[\text{Ox}_3] + ([\text{Ox}_4]_0/[\text{Ox}_2]_0)k_2([\text{Ox}_3]_0 - [\text{Ox}_3])[\text{Ox}_4]}$, $d[\text{Ox}_{n-1}]/dt = -([\text{Ox}_{n-1}]_0/[\text{Ox}_{n-2}]_0)k_2([\text{Ox}_{n-2}]_0 - [\text{Ox}_{n-2}])[\text{Ox}_{n-1}] + ([\text{Ox}_n]_0/[\text{Ox}_{n-2}]_0)k_2([\text{Ox}_{n-1}]_0 - [\text{Ox}_{n-1}])[\text{Ox}_n]$, $d[\text{Ox}_n]/dt = -([\text{Ox}_n]_0/[\text{Ox}_{n-2}]_0)k_2([\text{Ox}_{n-1}]_0 - [\text{Ox}_{n-1}])[\text{Ox}_n]$ where k_1 and k_2 are the electron transfer between the nearest redox site and the gold electrode, and the electron transfer between nearby redox sites in a single metal complex wire, respectively. $[\text{Ox}_i]_0$ and $[\text{Ox}_i]$ are the initial and present two-dimensional concentrations of the oxidized-form metal complex, respectively. In the case of a linear wire $\mathbf{A}^1(\text{FeL}^2)_n$,

$$[\text{Ox}_1] + [\text{Red}_1] = [\text{Ox}_2] + [\text{Red}_2] = \dots = [\text{Ox}_n] + [\text{Red}_n] = \text{constant} \quad (2)$$

In the case of a branched wire $\mathbf{A}^1(\text{FeL}^7)_n$,

$$[\text{Ox}_1] + [\text{Red}_1] = ([\text{Ox}_2] + [\text{Red}_2])/3 = \dots = ([\text{Ox}_n] + [\text{Red}_n])/(2^n - 1) = \text{constant} \quad (3)$$

The apparent current can be observed as $d[\text{Ox}_1]/dt$; however, the actual current contains the current decay derived from the double layer capacitance (C_{dl}), which decays exponentially. Thus, we used the sum of the $d[\text{Ox}_1]/dt$ decay and the C_{dl} decay as a theoretical curve.

In the simulation of $\mathbf{A}^1(\text{FeL}^2)_n$ ($n = 2, 4, 6, 8$) in 1 M $n\text{-Bu}_4\text{NClO}_4/\text{CH}_2\text{Cl}_2$, the simulated current decay curve with parameters $k_1 = (220 \pm 10) \text{ s}^{-1}$, $k_2 = (1.4 \pm 0.1) \times 10^{13} \text{ cm}^2 \text{ mol}^{-1} \text{ s}^{-1}$, and $C_{dl} = (25 \pm 10) \mu\text{C cm}^{-2}$ reproduced all of the experimental results well. The simulation of $\mathbf{A}^1(\text{FeL}^7)_n$ ($n = 2, 3, 4$) gave the parameters $k_1 = (260 \pm 10) \text{ s}^{-1}$, $k_2 = (4.8 \pm 0.2) \times 10^{12} \text{ cm}^2 \text{ mol}^{-1} \text{ s}^{-1}$, and $C_{dl} = (23 \pm 4) \mu\text{C cm}^{-2}$.

These simulations showed that the electron transfer occurred between the neighboring sites via the sequential electron hopping mechanism.

4.4. Long-range electron transport properties of bis(terpyridine) metal complex wires on Au

4.4.1. Introduction

The long-range electron transport abilities of molecular wires are one of their most attractive features in terms of their fundamental chemistry and molecular nanotechnology. It is believed that clarification of the electron transport mechanisms in molecular wires and the control of electron transfer kinetics will contribute to the development of molecule-based electronic devices. Therefore, many researchers have studied the charge transport and the conductivity of various molecular wires.

The long-range electron transport abilities are typically discussed in terms of the β value. There are two different methods for the estimation of the β value. One method uses the electron transfer rate constant (k_{ET}) from the electron donating group (D) to the electron accepting group (A). The D and A are separated by a molecular spacer (S). The other method uses the distance dependence of the molecular resistance. We will first explain how the β value can be estimated from k_{ET} .

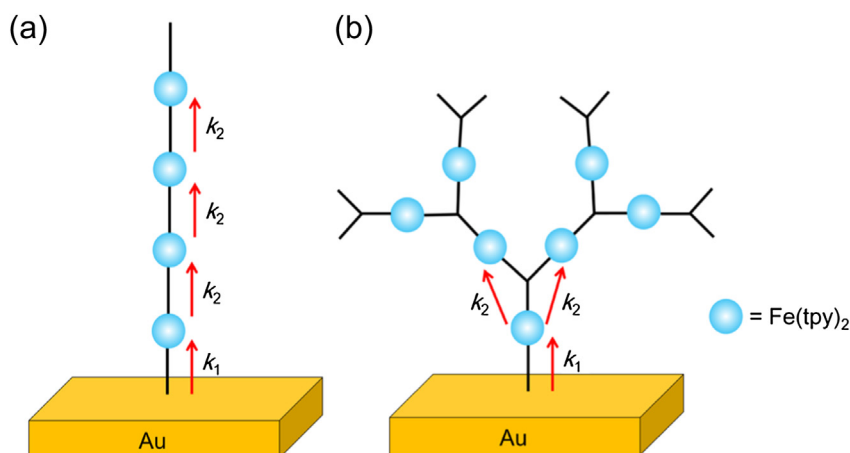


Fig. 11. Electron transport model within (a) a linear wire $\mathbf{A}^1(\text{FeL}^2)_n$ and (b) a branched wire $\mathbf{A}^1(\text{FeL}^7)_n$.

Two types of electron transfer mechanism have been proposed: superexchange and sequential hopping (Fig. 12). In the case of the superexchange mechanism, it is believed that the larger the interactions between the orbitals of D and A, the faster the k_{ET} , because the direct electron transfer from D to A occurs via tunneling. The k_{ET} is given as follows:

$$k_{ET} = k_0 \exp(-\beta d) \quad (4)$$

where d is the distance between D and A, and k_0 is the electron transfer rate constant when $d = 0$. From this equation, we can see that small β values result in a small decay in k_{ET} . Thus, molecular spacers with a small β value have good long-range electron transport abilities.

In the sequential hopping mechanism, the electron moves from D to A via the energy levels in S, and various explanations of the distance dependency of the electron transfer rate have been proposed. For example, Petrov et al. claimed that the k_{ET} decay is proportional to $1/N$ (N is the number of hopping sites), working from a theoretical prediction [165,166]. Kimura and coworkers measured the electron transfer rate constant of ferrocene linked to a gold electrode by various lengths of peptide chains using the AC impedance method, and investigated the relation between k_{ET} and d [167]. The authors hypothesized that this electron transfer mechanism was sequential hopping, and calculated the distance-dependency of k_{ET} theoretically. The estimated relation was different from Equation (4), but it corresponded well to the experimental results. However, in the case of the sequential hopping mechanism, the β value has mainly been used as a parameter for evaluating the long-range electron transport abilities, due to the lack of an established theory for sequential hopping, to enhance the reproducibility of experimental results, and for convenience when making comparisons among different molecular wires. In most cases, electron transfer that occurs via sequential hopping shows a weak dependence on distance.

The k_{ET} value of a surface-confined redox-active moiety can be estimated using electrochemical methods. Usually cyclic voltammetry, potential step chronoamperometry (PSCA), AC impedance methods (or electrochemical impedance spectroscopy, EIS), and AC voltammetry methods are used. Cyclic voltammetry is one of the most popular electrochemical analysis methods. The round-trip voltage is applied to a working electrode, and the current flow of a working electrode is recorded as a function of the potential. In the cyclic voltammogram of surface-confined redox species, the peak current is proportional to the scan rate. The determination of the k_{ET} value is performed according to the Laviron equation [168]. In order to estimate the k_{ET} value, the transfer coefficient α is needed, for which the ideal value is 0.5. The value of α is determined from a plot of the peak potential E_p as a function of $\log \nu$ (which is the scan rate used in the cyclic voltammetry). In the high-scan-rate region, a linear relation can be observed, and α is expressed as follows:

$$\alpha = s_a / (s_a - s_c) \quad (5)$$

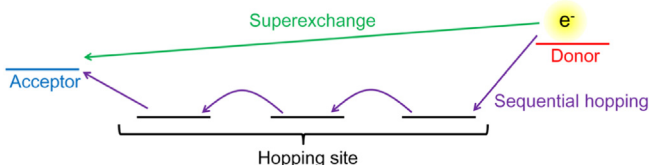


Fig. 12. Charge transport mechanisms.

where s_a and s_c are the slope of the anodic branch and the cathodic branch, respectively.

Once an α value is estimated, the cathodic k_{ET} value (k_c) and the anodic k_{ET} value (k_a) can be obtained as follows [169–173]:

$$k_c = (\alpha n F v_c) / (RT) \quad (6)$$

$$k_a = (1 - \alpha)(n F v_a) / (RT) \quad (7)$$

where v_c and v_a are the scan rate at the intersection points of the $\log \nu$ axis and the lines for the cathodic branch and the anodic branch, respectively (Fig. 13).

In PSCA, an overpotential is applied to a working electrode, and the current decay is recorded as a function of time. The relation between the current decay of the surface-immobilized redox species and time t is expressed as follows [174]:

$$I = I_0 \exp(-k_{ET} t) \quad (8)$$

where I_0 is the current at $t = 0$. The k_{ET} value at the applied overpotential can be estimated from the slope in the $\ln I - t$ plot (Fig. 14) [175–177].

When using the AC impedance method, the current response of a modified electrode to the input voltage signal is measured. By comparing the sine wave input and the response, the impedance and admittance of the electrode reaction are defined. The analysis is performed by fitting a theoretical equivalent circuit to the experimental result. The equivalent circuits shown in Fig. 15 can be used for the electron transfer rate constant analysis of surface-confined redox active moieties. Other equivalent circuits also can be used if they can explain the analyzed systems. A constant phase element (CPE) is sometimes used instead of a capacitance, because it reproduces the real electron transport system well. In the case of circuit (A), k_{ET} is given as follows [178]:

$$k_{ET} = 1 / (2R_{ET}C_{ET}) \quad (9)$$

On the other hand, the k_{ET} of circuit (B) is expressed as [179]:

$$k_{ET} = (RT) / (n^2 F^2 \Gamma R_{ET}) \quad (10)$$

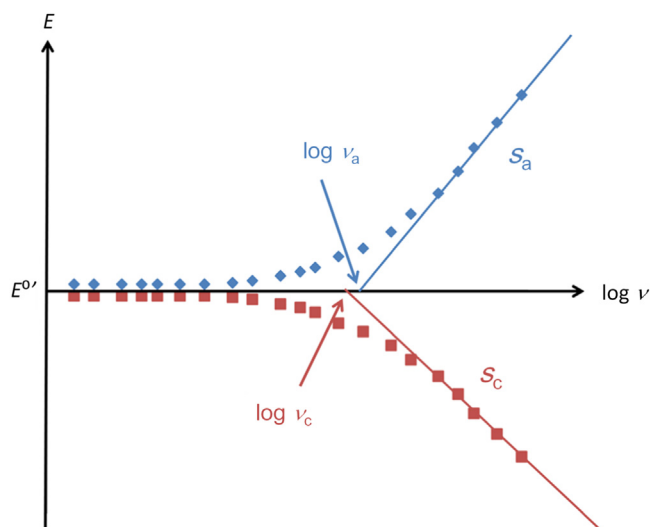


Fig. 13. Plot of the anodic and cathodic peak potentials vs. $\log \nu$. The blue dots show the anodic peak potentials, and the red dots show the cathodic peak potentials.

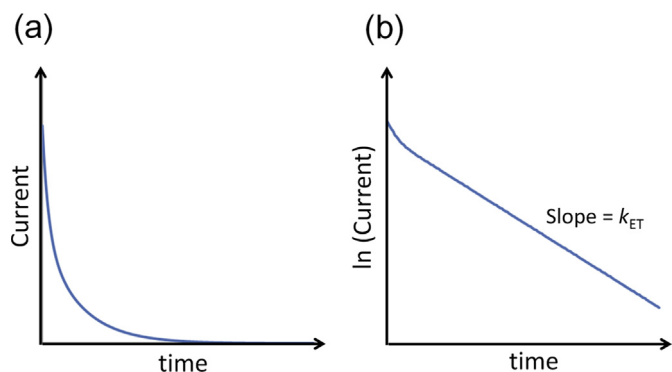


Fig. 14. Current decay behavior in potential step chronoamperometry. (a) Current–time plot. (b) $\ln I - t$ plot. The slope of the linear decay region in $\ln I - t$ plot gives the k_{ET} value.

where R_{ET} , C_{ET} , R , T , n , F , and Γ are the charge transfer resistance, the electron transfer capacitance, the gas constant, the temperature, the number of electrons involved in the charge transfer, the Faraday constant, and the surface coverage, respectively. The k_{ET} value at the redox potential ($E^{0'}$) can be obtained using the fitting of experimental results by the simulated curve [180–184].

The method for evaluating k_{ET} from AC voltammetry was developed by Creager et al. [185,186]. The AC voltammograms are collected at various frequencies, and a series of I_p/I_b ratios are plotted as a function of the common logarithm of the frequency. Here, I_p is the current at the peak top and I_b is the background current. This plot is fitted by the circuit (A) in Fig. 15. The parameters in the circuit (A), solvent resistance R_S , electron transfer resistance R_{CT} , electron transfer capacitance C_{CT} , and electronic double layer C_{dl} are written as follows:

$$R_S = 1/(4\pi r_0 K) \quad (11)$$

$$R_{CT} = (2RT)/(F^2 A \Gamma k_{ET}) \quad (12)$$

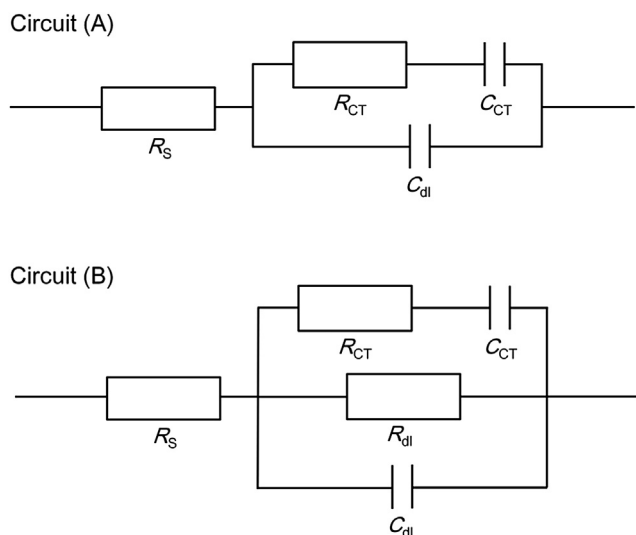


Fig. 15. Typical equivalent circuits for estimation of the k_{ET} value of SAMs using AC impedance and AC voltammetry.

$$C_{CT} = (F^2 A \Gamma)/(4RT) \quad (13)$$

$$C_{dl} = (C/A)A \quad (14)$$

The C_{dl} , Γ , A , and R_S parameters can be obtained from cyclic voltammetry, or using the AC impedance method. Therefore, the fitting for the determination of the k_{ET} value can be achieved using the two independent parameters R_{CT} and C_{dl} . This method has been used in a number of articles to obtain the k_{ET} values for redox-active SAMs [187–189].

The typical methods used to determine the β value from the resistance of a molecular wire are junction-breaking using STM [190–193], current sensing using AFM [194–197], metal contact [198–201], and conducting polymer contact [202–204] (Fig. 16). In these methods, the resistance values of various lengths of molecular wires are measured, and the relation between $\ln R$ and L is plotted, where R and L are the resistance and the length of the molecular wire, respectively. This relation is as follows:

$$R = R_0 \exp(\beta L) \quad (15)$$

Thus, the β value can be estimated from the slope of the $\ln R - L$ plot.

In recent studies, the β values of alkyl chains (0.36 – 0.93 \AA^{-1} , assuming 1.25 \AA along the chain per CH_2) [191,198–200,204], porphyrin (0.034 \AA^{-1}) [193], peptide chains (0.32 – 0.46 \AA^{-1}) [186,205], DNA (0.2 – 1.8 \AA^{-1}) [206–208], π -conjugated chains (0.02 – 0.034 \AA^{-1}) [190,192,197], oligophenylene (0.2 – 0.77 \AA^{-1}) [196,202], acenes (0.2 \AA^{-1} for monothiol, 0.5 \AA^{-1} for dithiol) [195], π -stacked benzenes (0.63 \AA^{-1}) [209], a viologen wire (0.006 \AA^{-1}) [210], and metal complexes (0.028 \AA^{-1} for $\text{Fe}(\text{tpy})_2$, 0.001 \AA^{-1} for $\text{Co}(\text{tpy})_2$, and 0.012 – 0.021 \AA^{-1} for Ru complex) [201,211] have been reported. In this section, the effects of the bridging unit, anchor ligand, and terminal ligand of $\text{M}(\text{tpy})_2$ complex wires on the β and k_{ET} values are discussed.

4.4.2. Effects of bridging units

Our $\text{M}(\text{tpy})_2$ metal complex wires were composed of three building blocks: an anchor ligand **A**, a bridging unit containing metal ions and bridging ligands **L**, and a terminal ligand **T**. It is important to understand how these components influence the electron transport properties to achieve the realization of molecule-based electron transfer systems. First, the effects of bridging ligands were researched. The **L**¹–**L**⁵ were used as a bis(terpyridine) bridging ligand, and Fe^{2+} was chosen as a metal ion. The **T**¹, **T**², or $\text{Co}(\text{tpy})_2$ complexes were immobilized at the termination of the $\text{Fe}(\text{tpy})_2$ metal complex wires. The β values of these $\text{Fe}(\text{tpy})_2$ complex wires were 0.008 – 0.07 \AA^{-1} (Table 4). Most of the values were in the range of $0.02 \pm 0.01 \text{ \AA}^{-1}$, showing enhanced long-range electron transport properties compared with known molecular wires. The $\text{Fe}(\text{tpy})_2$ wire bridged by **L**³ showed an exceptionally large β value of 0.07 \AA^{-1} . The **L**³ is an ethynylene moiety, which is a strong electron-withdrawing group, and the redox potential of **A**¹ FeL^3 (0.75 V vs. Fc^+/Fc) was higher than that of **A**¹ FeL^X , which contained a phenylene-based bridging ligand (e.g., 0.67 V for **L**¹, 0.61 V for **L**², and 0.63 V for **L**⁴ and **L**⁵). Therefore, it was concluded that the difference between the HOMO levels of the $\text{Fe}(\text{tpy})_2$ complex wire and **T**¹ became larger, and the highest β value was obtained.

The influence of the bridging ligand was investigated using a comparison between **A**¹(FeL^2) $n-1$ FeT^1 , **A**¹(FeL^4) $n-1$ FeT^2 , and **A**¹(FeL^5) $n-1$ FeT^1 (Fig. 17). The **A**¹(FeL^4) $n-1$ FeT^2 showed the smallest β value ($\beta = 0.008 \pm 0.006 \text{ \AA}^{-1}$), which meant that it also showed the best long-range electron transport abilities. The β value for **A**¹(FeL^2) $n-1$ FeT^1 was the second smallest ($\beta =$

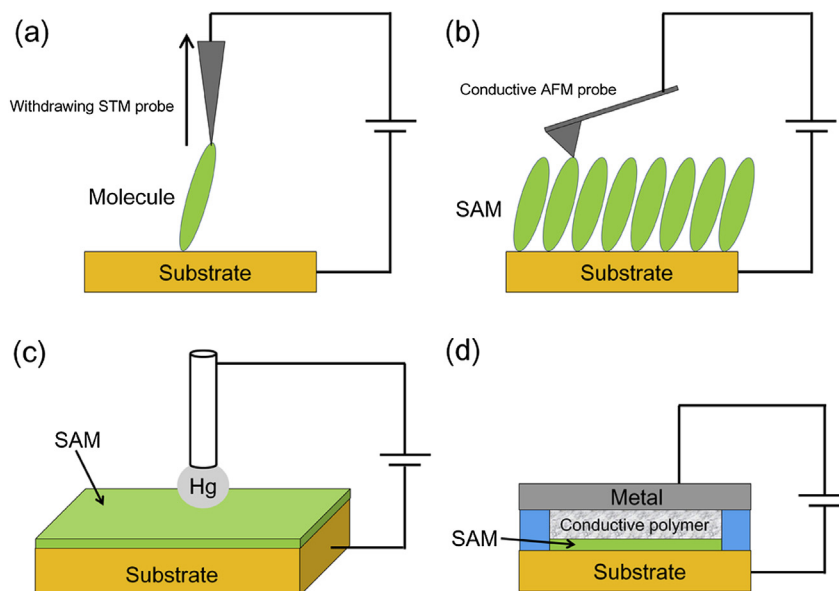


Fig. 16. Resistivity measurement methods for SAMs. (a) Junction-breaking method using STM, (b) conductive AFM, (c) metal contact method, and (d) conductive polymer contact.

$0.015 \pm 0.007 \text{ \AA}^{-1}$), and that of $\text{A}^1(\text{FeL}^5)_{n-1}\text{FeT}^1$ was the largest ($\beta = 0.031 \pm 0.008 \text{ \AA}^{-1}$). From these results, we were able to estimate the important factors affecting the β values. The first was the distance between the neighboring $\text{M}(\text{tpy})_2$ units. The electron transfer in the $\text{M}(\text{tpy})_2$ wires occurred via sequential hopping between the neighboring metal complexes. It is likely that the shorter distance yielded a smaller attenuation factor β , because it reduced the energy barriers between the nearest hopping sites and produced a higher electron hopping rate. The Fe–Fe distance bridged by L^2 was shorter than that bridged by L^5 . Therefore, the β value of the L^2 -bridged wire was smaller. However, this could not explain the excellent long-range electron transport abilities of $\text{A}^1(\text{FeL}^4)_{n-1}\text{FeT}^2$. Its bridging ligand L^4 had a longer Fe–Fe distance than L^2 . Thus, it is likely that other factors influenced the β value. In the case of L^4 , one possible influence was the molecular orbital of the bridging ligand. The dimethyldihydropyrene (DHP) redox peak in L^4 was observed at approximately $E^{0r} = 0.12 \text{ V}$ vs. Fc^+/Fc . This redox potential was close to the redox potential of T^2 . We formulated two hypotheses about the electron transport mechanism in the L^4 -bridged wires on the basis of the redox potential of DHP. The first proposed that a DHP moiety participated in the electron transport as a hopping site, and the second proposed that the DHP moiety accelerated the electron hopping within the wire via the enhancement of the electronic communication between the closest two $\text{Fe}(\text{tpy})_2$ complexes. Either process would encourage the electron transport between the terminal ferrocene moiety and the electrode. These results indicated that the electron transport abilities of the $\text{M}(\text{tpy})_2$ metal complex wires could be controlled by the bridging ligands.

Table 4
 β values of $\text{M}(\text{tpy})_2$ metal complex wires.

Wire	β value/ \AA^{-1}
$\text{A}^1(\text{FeL}^1)_n\text{CoL}^1$	0.012 ± 0.001
$\text{A}^1(\text{FeL}^2)_{n-1}\text{FeT}^1$	0.015 ± 0.007
$\text{A}^1(\text{FeL}^3)_{n-1}\text{FeT}^1$	0.07 ± 0.02
$\text{A}^1(\text{FeL}^4)_{n-1}\text{FeT}^2$	0.008 ± 0.006
$\text{A}^1(\text{FeL}^5)_{n-1}\text{FeT}^1$	0.031 ± 0.008
$\text{A}^1(\text{CoL}^1)_n\text{FeL}^1$	0.002 ± 0.001
$\text{A}^1(\text{CoL}^2)_n\text{FeL}^2$	0.004 ± 0.002

In order to assess the effects of metal ions in the $\text{M}(\text{tpy})_2$ complex wires on the β value, we fabricated cobalt complex wires, $\text{A}^1(\text{CoL}^1)_n\text{FeL}^1$ and $\text{A}^1(\text{CoL}^2)_n\text{FeL}^2$. The redox current decay of $[\text{Fe}(\text{tpy})]^{3+/2+}$ was monitored using the PSCA method to estimate the electron transfer rate from the $\text{Fe}(\text{tpy})_2$ complexes. The $\text{A}^1(\text{CoL}^1)_n\text{FeL}^1$ and $\text{A}^1(\text{CoL}^2)_n\text{FeL}^2$ exhibited β values of $0.002 \pm 0.001 \text{ \AA}^{-1}$ and $0.004 \pm 0.002 \text{ \AA}^{-1}$, respectively (Table 4). These values were smaller than those of the $\text{Fe}(\text{tpy})_2$ complex wires. In fact, the $\text{Co}(\text{tpy})_2$ complex wires had enhanced long-range electron transport abilities. These results showed that one could change the electron transport abilities of $\text{M}(\text{tpy})_2$ wires via the incorporation of metal ions.

The dependency of the β value on the measurement and ambient conditions was investigated. The β value of $\text{A}^1(\text{FeL}^2)_{n-1}\text{FeT}^1$ was almost independent of the overpotential, electrolyte concentration, and temperature, and could be expressed as $0.02 \pm 0.01 \text{ \AA}^{-1}$. These results suggested that the long-range electron transport occurred without any migration of the counterions, and that the β value was the intrinsic parameter of the metal complex wire. However, the k_{ET} values showed a strong dependency on the measurement conditions.

The thermodynamic parameters of $\text{A}^1(\text{FeL}^2)_{n-1}\text{FeT}^1$ were determined as $E_a = 10.5\text{--}12.8 \text{ kJ mol}^{-1}$, $\Delta H = 8.5\text{--}10.9 \text{ kJ mol}^{-1}$, and $\Delta S = -151 \text{ to } -164 \text{ J mol}^{-1}\text{K}^{-1}$ from the dependence of the k_{ET} values on the temperature, and all of the parameters showed a slight dependence on the length of the metal complex wire. As a typical system that transports electrons via the superexchange mechanism, the thermodynamic parameters of $\text{FcCO}_2(\text{CH}_2)_n\text{SH}$ ($n = 8, 12, 16$) SAMs have been estimated using the electrochemical method (Table 5) [212]. Compared with the parameters of the ferrocenyl SAMs, $\text{A}^1(\text{FeL}^2)_{n-1}\text{FeT}^1$ showed smaller values. The small activation energy and the small dependence on the wire length suggested that the electron transport mechanism in metal complex molecular wires is sequential hopping.

4.4.3. Potential-gradient metal complex wires

Molecular wires that have a potential gradient are attractive, because the presence of potential steps can control the direction of the electron transport, and they enable extremely fast and effective electron transport. For example, a photosynthesis system uses a

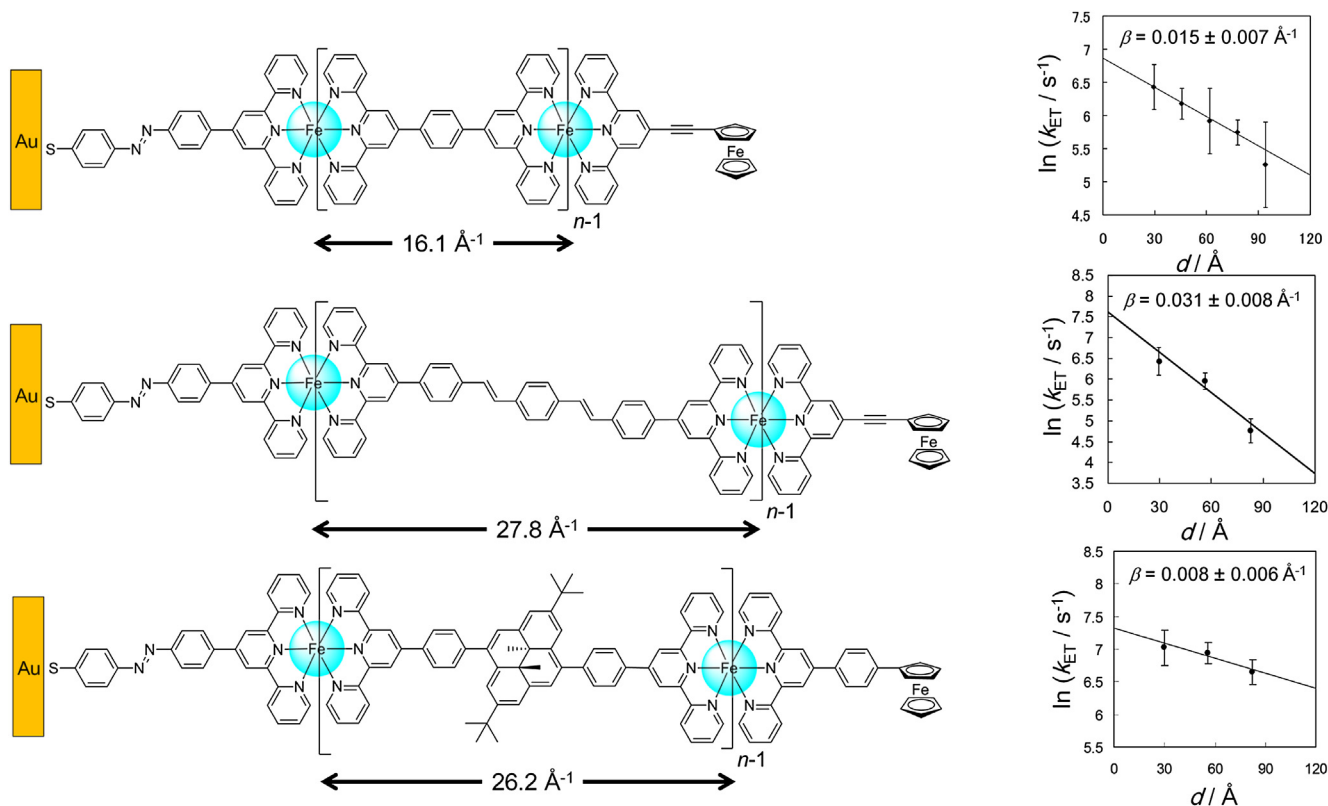


Fig. 17. Structures of $A^1(FeL^2)_{n-1}FeT^1$, $A^1(FeL^5)_{n-1}FeT^1$, and $A^1(FeL^4)_{n-1}FeT^2$, and their $\ln k_{ET} - d$ plots. Adapted with permission from Ref. [213]. Copyright (2012) Elsevier.

potential gradient to achieve highly efficient photo-electron conversion. We introduced a potential gradient to the metal complex wires using two species of metal ions (Fe^{2+} , Co^{3+}) and ligands (L^2 , L^3), and evaluated their electron transport behaviors.

The $A^1FeL^2CoT^1$ and $A^1CoL^2FeT^1$ were prepared on a gold electrode using the stepwise coordination method. Their k_{ET} values were estimated using the PSCA method, and the k_{ET} of $A^1CoL^2FeT^1$ was larger than that of $A^1FeL^2CoT^1$. This phenomenon can be explained by the fact that the oxidation reaction of T^1 was more effectively mediated by the electron transfer to $Co(tpy)_2$ than that to $Fe(tpy)_2$.

The $A^2FeL^2(FeL^2)_2$ and $A^2FeL^3(FeL^2)_2$ were fabricated as gradient wires with an inherent potential. The overlapped redox peaks of these complex wires were observed in the range from 0.6 to 0.8 V vs. Fc^+/Fc , because the redox potential of the $Fe(tpy)_2$ complex was shifted higher by the introduction of fluorinated terpyridine. The PSCA results for $A^2FeL^2(FeL^2)_2$ revealed that the reduction current was larger than the oxidation current. This observation agreed with the expectation from the potential gradient in $A^2FeL^2(FeL^2)_2$. However, $A^2FeL^3(FeL^2)_2$ also showed a

Table 5
Thermodynamic parameters of $A^1(FeL^2)_{n-1}FeT^1$ and $FcCO_2(CH_2)_nSH$ SAMs on a gold electrode.

	$E_a/kJ\ mol^{-1}$	$\Delta H/kJ\ mol^{-1}$	$\Delta S/JK^{-1}mol^{-1}$	$d/\text{\AA}^{-1}$
A^1FeT^1	12.8	10.9	-151	29.6
$A^1(FeL^2)_1FeT^1$	11.7	9.77	-158	45.7
$A^1(FeL^2)_2FeT^1$	11.9	9.92	-158	61.8
$A^1(FeL^2)_3FeT^1$	10.5	8.53	-164	77.9
$A^1(FeL^2)_4FeT^1$	11.2	9.19	-162	94.0
$FcCO_2(CH_2)_8SH$	24.0	22.9	-88.9	15.6
$FcCO_2(CH_2)_{12}SH$	22.0	20.8	-137	20.8
$FcCO_2(CH_2)_{16}SH$	19.7	18.6	-189	26.0

reduction current that was slightly larger than the oxidation current, in spite of its inversed potential gradient. We believe that a significant difference wasn't observed because of the slow electron transfer at the electrode-molecular wire junction, and the fact that the reduction reaction was faster than the oxidation reaction at the same absolute overpotential.

4.4.4. Effect of surface anchor ligands

Anchor ligands play an important role as a junction between the electrode and the surface-confined molecular wires, so it is important to understand how anchor ligands affect the electron transfer properties from the viewpoint of the electronic property control of molecular systems. The $Fe(tpy)_2$ metal complex wires with T^1 terminal ligands were constructed on three types of anchor ligands: A^1 , A^2 , or A^3 , and the relation between $\ln k_{ET}$ and d was

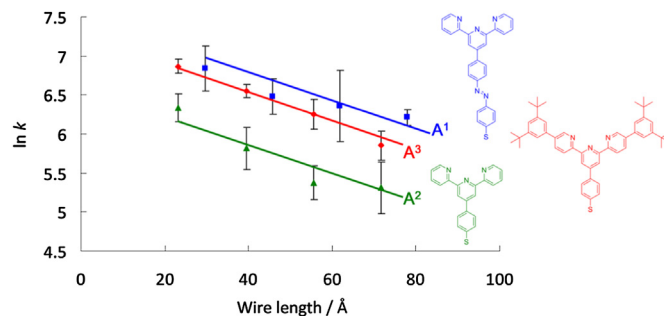


Fig. 18. $\ln k_{ET} - d$ plots of $A^1(FeL^2)_{n-1}FeT^1$ (blue dots and line), $A^2(FeL^2)_{n-1}FeT^1$ (green dots and line), and $A^3(FeL^2)_{n-1}FeT^1$ (red dots and line). The error bars show the standard deviation of each measurement point. The solid lines show the fitting results determined using the weighted least squares method. Adapted with permission from Ref. [149]. Copyright (2010) American Chemical Society.

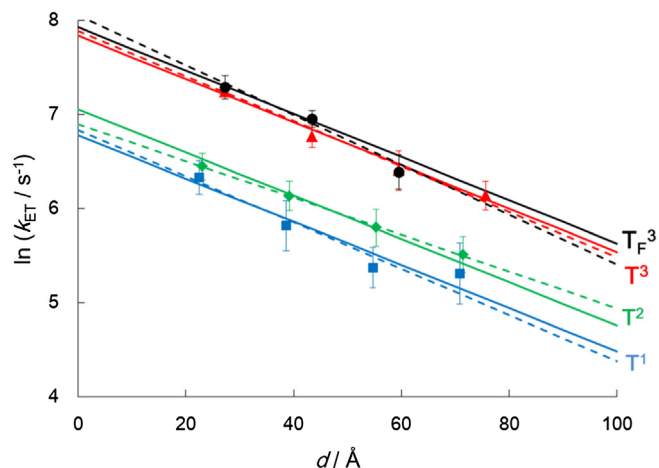


Fig. 19. In $k_{\text{ET}} - d$ plots of $\text{A}^2(\text{FeL}^2)_{n-1}\text{FeT}^1$ (blue dots and line), $\text{A}^2(\text{FeL}^2)_{n-1}\text{FeT}^2$ (green dots and line), $\text{A}^1(\text{FeL}^2)_{n-1}\text{FeT}^3$ (red dots and line), and $\text{A}^1(\text{FeL}^2)_{n-1}\text{FeT}^2$ (black dots and line). The error bars show the standard deviation of each measurement point. The dashed lines show the fitting results determined using the weighted least squares method, and the solid lines show the slope of $\beta = 0.023 \text{ \AA}^{-1}$. From Ref. [151]. Copyright © 2007 by John Wiley & Sons, Inc. Reprinted by permission of John Wiley & Sons, Inc.

plotted (Fig. 18). The electron transfer kinetics were dependent on anchor ligands, whereas the β value was independent, with a value of $\beta = 0.018 \text{ \AA}^{-1}$. This result showed that an anchor ligand mainly affects the electron transfer rate. The differences in the k_{ET}^0 values of the terminal ferrocene moieties could be described in terms of the molecular orbital of A^1 and the steric effects of the *t*-Bu₂Ph group of A^3 . A^1 had a molecular orbital extending over the anchor atom, S, azobenzene, and the metal center, Fe^{II}. It is likely that this orbital enhanced the electric interactions between the Fe(tpy)₂ complexes and the gold electrode, and accelerated the electron transport. In the case of A^3 , electrolyte ions could easily approach the redox center of the Fe(tpy)₂ complexes, due to the bulky structure of A^3 . According to the comparison between A^2FeL^2 and A^3FeL^2 , A^3FeL^2 showed a higher electron transfer rate constant (330 s^{-1}) than A^2FeL^2 (56 s^{-1}).

4.4.5. Influence of terminal ligands

Finally, the effects of the terminal ligands were researched. We used T^1 – T^3 and T^3 as terminal ligands, and A^2 was used as a surface anchor ligand. From one- to three- or four-layer Fe(tpy)₂ metal complex wires were fabricated, and the relation between k_{ET} and the molecular length was determined. As shown in Fig. 19, the β value of the metal complex wires was constant ($\beta = 0.023 \text{ \AA}^{-1}$),

while the k_{ET}^0 values were affected by the terminal ligands. This result suggested that the terminal ligands strongly influenced the electron transfer rate, rather than the long-range electron transport properties. The difference between the k_{ET}^0 values for T^2 and T^3 was especially distinct. In order to fully understand this phenomenon, the reorganization energy (λ) values for the ferrocene and ruthenium complexes (**Ru1**, Fig. 20) were estimated using AC voltammetry in a 1 M *n*-Bu₄NClO₄/CH₂Cl₂ solution. The values were obtained as $0.53 \pm 0.04 \text{ eV}$ for ferrocene and $0.43 \pm 0.05 \text{ eV}$ for **Ru1**, respectively. We therefore believe that the larger k_{ET}^0 value of T^3 derived from its smaller λ value, because of the bulkiness of the cyclometallated ruthenium complex.

5. Conclusion

This review focused on the stepwise synthesis of metal complex oligomer and polymer wires on metal, semiconductor, and insulating surfaces; on the evaluation of the methods and functions associated with these wires; and on the electrochemical properties of our bis(terpyridine) metal complex wire system. Various combinations of metal ions, metal complexes, metal clusters, and bridging ligands were used to prepare metal complex wires, and to generate functions including catalytic activity and photocurrent generation. Not only linear metal complex wires but also branched structures and network structures were constructed, using ligands with three coordination sites and carbon nanotubes, respectively. The electrochemical measurements of our M(tpy)₂ wires provided insight into the electron transfer behavior of metal complex wire systems in which redox sites are arranged regularly, and into the dependence of the long-range electron transport properties on the building blocks for the M(tpy)₂ wires, the anchor ligands, the bridging ligands or metal ions, and the terminal ligands. Very small β values were observed in $\text{A}^1(\text{FeL}^4)_{n-1}\text{FeT}^2$ ($\beta = 0.008 \pm 0.006 \text{ \AA}^{-1}$) and $\text{A}^1(\text{CoL}^1)_n\text{FeL}^1$ ($\beta = 0.002 \pm 0.001 \text{ \AA}^{-1}$), and thermodynamic analysis suggested that the electron transport phenomena in this metal complex wire system occurred via the sequential hopping mechanism. Metal complex wires have advantages in the fact that their properties can be controlled by varying the combination of metal ions and ligands, and that they can be constructed using simple methods. These benefits will allow us to develop molecular electric devices via the introduction of functional molecules with photoresponsivity, magnetic properties, and stimuli response within metal complex wires. The topic treated in this review will contribute to the realization of molecule-based electronics and the progression of the nanotechnology field.

References

- [1] Whalley AC, Steigerwald ML, Guo X, Nuckolls C. *J Am Chem Soc* 2007;129:12590–1.
- [2] Díez-Pérez I, Hihath J, Lee Y, Yu L, Adamska L, Kozhushner MA, et al. *Nat Chem* 2009;1:635–41.
- [3] Ballesteros LM, Martin S, Pera G, Schauer PA, Kay NJ, López MC, et al. *Langmuir* 2011;27:3600–10.
- [4] Ribena D, Alekseev A, van Asselen O, Mannie GJA, Hendrix MMRM, van der Ven LGJ, et al. *Langmuir* 2012;28:16900–8.
- [5] Zhang S, Wang H-L, Chen M, Qian D-J. *Colloid Surf A* 2011;384:561–9.
- [6] Nie H-J, Shao J-Y, Wu J, Yao J, Zhong Y-W. *Organometallics* 2012;31:6952–9.
- [7] Nalin de Silva KM, Hwang E, Serem WK, Fronczek FR, Garno JC, Nesterov EE. *ACS Appl Mater Interfaces* 2012;4:5430–41.
- [8] Xu W, Wang J, Yu M, Laegsgaard E, Stensgaard I, Linderorth TR, et al. *J Am Chem Soc* 2010;132:15927–9.
- [9] Montero L, Baxamusa SH, Borros S, Gleason KK. *Chem Mater* 2009;21:399–403.
- [10] Xu M, Liang T, Shi M, Chen H. *Chem Rev*, <http://dx.doi.org/10.1021/cr300263a>.
- [11] Tian H, Dai Y, Shao H, Yu H-Z. *J Phys Chem C* 2013;117:1006–12.
- [12] Singhana B, Rittikulsittichai S, Lee TR. *Langmuir* 2013;29:561–9.

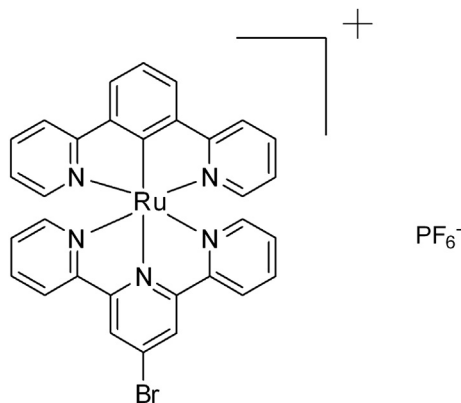


Fig. 20. Structure of compound **Ru1**.

- [13] Gatto E, Porchetta A, Scarselli M, Crescenzi MD, Formaggio F, Toniolo C, et al. *Langmuir* 2012;28:2817–26.
- [14] Breuer R, Schmittel M. *Organometallics* 2012;31:6642–51.
- [15] Ahmad A, Moore E. *Analyst* 2012;137:5839–44.
- [16] Muglali MI, Liu J, Bashir A, Borissov D, Xu M, Wang Y, et al. *Phys Chem Chem Phys* 2012;14:4703–12.
- [17] Cizek JW, Stewart MP, Tour JM. *J Am Chem Soc* 2004;126:13172–3.
- [18] Shen C, Buck M, Wilton-Ely JDET, Weidner T, Zharnikov M. *Langmuir* 2008;24:6609–15.
- [19] Valkenier H, Huisman EH, van Hal PA, de Leeuw DM, Chiechi RC, Hummelen JC. *J Am Chem Soc* 2011;133:4930–9.
- [20] Ford K, Battersby BJ, Wood BJ, Gentle IR. *J Colloid Interf Sci* 2012;370:162–9.
- [21] Cormode DP, Evans AJ, Davbis JJ, Beer PD. *Dalton Trans* 2010;39:6532–41.
- [22] Takamatsu D, Fukui K, Aroua S, Yamakoshi Y. *Org Biomol Chem* 2010;8:3655–64.
- [23] Yamamoto K, Sugiura H, Amemiya R, Aikawa H, An Z, Yamaguchi M, et al. *Tetrahedron* 2011;67:5972–8.
- [24] Wang X, Fukuoka S, Tsukigawara R, Nagata K, Higuchi M. *J Colloid Interf Sci* 2013;390:54–61.
- [25] Sander F, Hermes JP, Mayor M, Hamoudi H, Zharnikov M. *Phys Chem Chem Phys* 2013;15:2836–46.
- [26] Petrovykh DY, Kimura-Suda H, Opdahl A, Richter LJ, Tarlov MJ, Whitman LJ. *Langmuir* 2006;22:2578–87.
- [27] Bong D, Tam I, Breslow R. *J Am Chem Soc* 2004;126:11796–7.
- [28] Li C, Ren B, Zhang Y, Cheng Z, Liu X, Tong Z. *Langmuir* 2008;24:12911–8.
- [29] Rampulla DM, Wroge CM, Hanson EL, Kushmerick JG. *J Phys Chem C* 2010;114:20852–5.
- [30] Polaske NW, Lin H-C, Tang A, Mayukh M, Oquendo LE, Green JT, et al. *Langmuir* 2011;27:14900–9.
- [31] Matsuo Y, Ichiki T, Nakamura E. *J Am Chem Soc* 2011;133:9932–7.
- [32] Hwang E, Nalin de Silva KM, Seevers CB, Li J-R, Garno JC, Nesterov EE. *Langmuir* 2008;24:9700–6.
- [33] Namiki K, Sakamoto A, Murata M, Kume S, Nishihara H. *Chem Commun* 2007:4650–2.
- [34] Miyachi M, Ohta M, Nakai M, Kubota Y, Yamanoi Y, Yonezawa T, et al. *Chem Lett* 2008;37:404–5.
- [35] Caro AM, Armini S, Richard O, Maes G, Borghs G, Whelan CM, et al. *Adv Funct Mater* 2010;20:1125–31.
- [36] Ramin MA, Bourdon GL, Heuzé K, Degueil M, Belin C, Buffeteau T, et al. *Langmuir* 2012;28:17672–80.
- [37] Walter SR, Youn J, Emery JD, Kewalramani S, Hennek JW, Bedzyk MJ, et al. *J Am Chem Soc* 2012;134:11726–33.
- [38] Gnanappa AK, O'Murchu C, Slattery O, Peters F, O'Hara T, Aszalós-Kiss B, et al. *Appl Surf Sci* 2011;257:4331–8.
- [39] Hayashi K, Sugimura H, Takai O. *Jpn J Appl Phys* 2001;40:4344–8.
- [40] Buriak JM. *ChemComm* 1999:1051–60.
- [41] Wayner DDM, Wolkow RA. *J Chem Soc Perkin Trans* 2002;2:23–34.
- [42] Sano H, Maeda H, Ichii T, Murase K, Noda K, Matsushige K, et al. *Langmuir* 2009;25:5516–25.
- [43] Seitz O, Dai M, Aguirre-Tostado FS, Wallace RM, Chabal YJ. *J Am Chem Soc* 2009;131:18159–67.
- [44] Sano H, Ohno K, Ichii T, Murase K, Sugimura H. *Jpn J Appl Phys* 2010;49:01AE09.
- [45] Song JH, Sailor MJ. *J Am Chem Soc* 1998;120:2376–81.
- [46] Song JH, Sailor MJ. *Inorg Chem* 1999;38:1498–503.
- [47] Ciampi S, Harper JB, Gooding JJ. *Chem Soc Rev* 2010;39:2158–83.
- [48] Liu Y, Yamazaki S, Yamabe S, Nakato Y. *J Mater Chem* 2005;15:4906–13.
- [49] Sun Q-Y, de Smet LCPM, van Lagen B, Wright A, Zuillhof H, Sudhölter EJR. *Angew Chem Int Ed* 2004;43:1352–5.
- [50] Huck LA, Buriak JM. *Langmuir* 2012;28:16285–93.
- [51] Eves BJ, Lopinski GP. *Surf Sci* 2005;579:89–96.
- [52] Salingue N, Hess P. *Appl Phys A-Mater* 2011;104:987–91.
- [53] Shestopalov AA, Morris CJ, Vogen BN, Hoertz A, Clark RL, Toone EJ. *Langmuir* 2011;27:6478–85.
- [54] Rohde RD, Agnew HD, Yeo W-S, Bailey RC, Heath JR. *J Am Chem Soc* 2006;128:9518–25.
- [55] Tian F, Taber DF, Teplyakov AV. *J Am Chem Soc* 2011;133:20769–77.
- [56] Gowda S, Mathur G, Misra V. *Appl Phys Lett* 2007;90:142113.
- [57] Hauquier F, Ghilane J, Fabre B, Hapiot P. *J Am Chem Soc* 2008;130:2748–9.
- [58] Sano H, Zhao M, Kasahara D, Murase K, Ichii T, Sugimura H. *J Colloid Interf Sci* 2011;361:259–69.
- [59] Feng W, Miller B. *Langmuir* 1999;15:3152–6.
- [60] Wrighton MS, Austin RG, Bocarsly AB, Bolts JM, Hass O, Legg KD, et al. *J Am Chem Soc* 1978;100:1602–3.
- [61] Zhang S, Koberstein JT. *Langmuir* 2012;28:486–93.
- [62] Morris CJ, Shestopalov AA, Gold BH, Clark RL, Toone EJ. *Langmuir* 2011;27:6486–9.
- [63] Ardalan P, Sun Y, Pianetta P, Musgrave CB, Bent SF. *Langmuir* 2010;26:8419–29.
- [64] Ardalan P, Musgrave CB, Bent SF. *Langmuir* 2009;25:2013–25.
- [65] Knapp D, Brunschwig BS, Lewis NS. *J Phys Chem C* 2010;114:12300–7.
- [66] Knapp D, Brunschwig BS, Lewis NS. *J Phys Chem C* 2011;115:16389–97.
- [67] Xu FJ, Cai QJ, Kang ET, Neoh KG, Zhu CX. *Organometallics* 2005;24:1768–71.
- [68] Holmberg VC, Korgel BA. *Chem Mater* 2010;22:3698–703.
- [69] Han SM, Ashurst WR, Carraro C, Maboudian R. *J Am Chem Soc* 2001;123:2422–5.
- [70] Hoeb M, Auernhammer M, Schoell SJ, Brandt MS, Garrido JA, Stutzmann M, et al. *Langmuir* 2010;26:18862–7.
- [71] Stenehjem ED, Ziatdinov VR, Stack TDP, Chidsey CED. *J Am Chem Soc* 2013;135:1110–6.
- [72] Strother T, Knickerbocker T, Russell Jr JN, Butler JE, Smith LM, Hamers RJ. *Langmuir* 2002;18:968–71.
- [73] Nakamura T, Suzuki M, Ishihara M, Ohana T, Tanaka A, Koga Y. *Langmuir* 2004;20:5846–9.
- [74] Knickerbocker T, Strother T, Schwartz MP, Russell Jr JN, Butler J, Smith LM, et al. *Langmuir* 2003;19:1938–42.
- [75] Lockett MR, Smith LM. *Langmuir* 2009;25:3340–3.
- [76] Lockett MR, Smith LM. *J Phys Chem C* 2010;114:12635–41.
- [77] Lockett MR, Smith LM. *Langmuir* 2010;26:16642–6.
- [78] Jouikov V, Simonet J. *Langmuir* 2012;28:931–8.
- [79] Lorcay D, Shin K-S, Guerro M, Simonet J. *Electrochim Acta* 2013;89:784–91.
- [80] Camacho-Alanis F, Castaneda H, Zangari G, Swami NS. *Langmuir* 2011;27:11273–7.
- [81] Arudra P, Marshall GM, Liu N, Dubowski JJ. *J Phys Chem C* 2012;116:2891–5.
- [82] Zhou C, Trionfi A, Jones JC, Hsu JWP, Walker AV. *Langmuir* 2010;26:4523–8.
- [83] McGuinness CL, Diehl GA, Blasini D, Smilgies D-M, Zhu M, Samarth N, et al. *ACS Nano* 2010;4:3447–65.
- [84] Alarcón LS, Chen L, Esaulov VA, Gayone JE, Sánchez EA, Grizzi O. *J Phys Chem C* 2010;114:19993–9.
- [85] Yamamoto H, Butera RA, Gu Y, Waldeck DH. *Langmuir* 1999;15:8640–4.
- [86] Lim H, Carraro C, Maboudian R, Pruessner MW, Ghodssi R. *Langmuir* 2004;20:743–7.
- [87] Franking R, Hamers RJ. *J Phys Chem C* 2011;115:17102–10.
- [88] Brown DG, Schauer PA, Borau-Garcia J, Fancy BR, Berlinguette CP. *J Am Chem Soc* 2013;135:1692–5.
- [89] Paz Y, Beilstein J. *Nanotechnol* 2011;2:845–61.
- [90] Hauffman T, Hubin A, Terryn H. *Surf Interface Anal* 2012. <http://dx.doi.org/10.1002/sia.5150>.
- [91] Yildirim O, Gang T, Kinge S, Reinholdt DN, Blank DHA, van der Wiel WG, et al. *Int J Mol Sci* 2010;11:1162–79.
- [92] Fukuda K, Hamamoto T, Yokota T, Sekitani T, Zschieschang U, Klauk H, et al. *Appl Phys Lett* 2009;95:203301.
- [93] Steenackers M, Sharp ID, Larsson K, Hutter NA, Stutzmann M, Jordan R. *Chem Mater* 2010;22:272–8.
- [94] Rosso M, Giesbers M, Arafat A, Schroën K, Zuillhof H. *Langmuir* 2009;25:2172–80.
- [95] Rosso M, Arafat A, Schroën K, Giesbers M, Roper CS, Maboudian R, et al. *Langmuir* 2008;24:4007–12.
- [96] Petoral Jr RM, Yazdi GR, Lloyd Spetz A, Yakimova R, Uvdal K. *Appl Phys Lett* 2007;90:223904.
- [97] Mahouche-Chergui S, Gam-Derouich S, Mangeney C, Chehimi MM. *Chem Soc Rev* 2011;40:4143–66.
- [98] Pinson J, Podvorica F. *Chem Soc Rev* 2005;34:429–39.
- [99] Bernard M-C, Chaussé A, Cabet-Deliry E, Chehimi MM, Pinson J, Prodvorica F, et al. *Chem Mater* 2003;15:3450–62.
- [100] Yang N, Zhuang H, Hoffmann R, Smirnov W, Hees J, Jiang X, et al. *Anal Chem* 2011;83:5827–30.
- [101] Civit L, El-Zubir O, Fragoso A, O'Sullivan CK. *Biosens Bioelectron* 2013;41:840–3.
- [102] Santos L, Ghilane J, Lacroix JC. *J Am Chem Soc* 2012;134:5476–9.
- [103] Flavel BS, Gross AJ, Garrett DJ, Nock V, Downard AJ. *ACS Appl Mater Interfaces* 2010;2:1184–90.
- [104] Le XT, Zeb G, Jégou P, Berthelot T. *Electrochim Acta* 2012;71:66–72.
- [105] Chen X, Chockalingam M, Liu G, Luais E, Gui AL, Gooding JJ. *Electroanal* 2011;23:2633–42.
- [106] Tascia F, Harreither W, Ludwig R, Gooding JJ, Gorton L. *Anal Chem* 2011;83:3042–9.
- [107] Boland S, Foster K, Leech D. *Electrochim Acta* 2009;54:1986–91.
- [108] Stewart MP, Maya F, Kosyunkin DV, Dirk SM, Stapleton JJ, McGuinness CL, et al. *J Am Chem Soc* 2004;126:370–8.
- [109] Jin Z, McNicholas TP, Shih C-J, Wang QH, Paulus GLC, Hilmer AJ, et al. *Chem Mater* 2011;23:3362–70.
- [110] Shewchuk DM, McDermott MT. *Langmuir* 2009;25:4556–63.
- [111] Lin S, Lin C-W, Jhang J-H, Hung W-H. *J Phys Chem C* 2012;116:17048–54.
- [112] March G, Reisberg S, Piro B, Pham M-C, Fave C, Noel V. *Anal Chem* 2010;82:3523–30.
- [113] Anariba F, DuVall SH, McCreery RL. *Anal Chem* 2003;75:3837–44.
- [114] Palomaki PKB, Krawicz A, Dinolfo PH. *Langmuir* 2011;27:4613–22.
- [115] Choi SH, Kim B, Frisbie CD. *Science* 2008;320:1482–6.
- [116] Antunes JC, Pereira CL, Molinos M, Ferreira-de-Silva F, Dessi M, Gloria A, et al. *Biomacromolecules* 2011;12:4183–95.
- [117] Liatard S, Chauvin J, Balestro F, Jouvenot D, Loiseau F, Deronzier A. *Langmuir* 2012;28:10916–24.
- [118] Gao S, Yuan D, Lü J, Li T, Cao R. *Chem Commun* 2007:1813–5.
- [119] Altman M, Shukla AD, Zubkov T, Evmenenko G, Dutta P, van der Boon ME. *J Am Chem Soc* 2006;128:7374–82.

- [120] Kosbar L, Srinivasan C, Afzali A, Graham T, Copel M, Krusin-Elbaum L. *Langmuir* 2006;22:7631–8.
- [121] Oo L, Kitamura F. *J Electroanal Chem* 2008;619–620:187–92.
- [122] Kanaizuka K, Haruki R, Sakata O, Yoshimoto M, Akita Y, Kitagawa H. *J Am Chem Soc* 2008;130:15778–9.
- [123] Shida A, Sugimura H, Futsuhara M, Takai O. *Surf Coat Tech* 2003;169–170:686–90.
- [124] Sugimura H, Yonezawa H, Asai S, Sun Q-W, Ichii T, Lee K-H, et al. *Colloid Surf A* 2008;321:249–53.
- [125] Tuccitto N, Delfanti I, Torrisi V, Scandola F, Chiorboli C, Stepanenko V, et al. *Phys Chem Chem Phys* 2009;11:4033–8.
- [126] Gao S, Huang Y, Cao M, Liu T, Cao R. *J Mater Chem* 2011;21:16467–72.
- [127] Mondal PC, Lakshmanan JY, Hamoudi H, Zharnikov M, Gupta T. *J Phys Chem C* 2011;115:16398–404.
- [128] Driscoll PF, Douglass Jr EF, Phewluangdee M, Soto ER, Cooper CGF, MacDonald JC, et al. *Langmuir* 2008;24:5140–5.
- [129] Liu J, Chen M, Qian D-J. *Langmuir* 2012;28:9496–505.
- [130] Pan Y, Tong B, Shi J, Zhao W, Shen J, Zhi J, et al. *J Phys Chem C* 2010;114:8040–7.
- [131] Abdelrazzaq FB, Kwong RC, Thompson ME. *J Am Chem Soc* 2002;124:4796–803.
- [132] Shekhah O, Wang H, Strunskus T, Cyganik P, Zacher D, Fischer R, et al. *Langmuir* 2007;23:7440–2.
- [133] Wanunu M, Vaskevich A, Cohen SR, Cohen H, Arad-Yellin R, Shanzler A, et al. *J Am Chem Soc* 2005;127:17877–87.
- [134] Chen H-T, Liu B, Wang H-T, Xiao Z-D, Chen M, Qian D-J. *Mater Sci Eng C* 2007;27:639–45.
- [135] Wanunu M, Popovitz-Biro R, Cohen H, Vaskevich A, Rubinstein I. *J Am Chem Soc* 2005;127:9207–15.
- [136] Langhals H. *Heterocycles* 1995;40:477–500.
- [137] Facchetti A. *Mater Today* 2007;10:28–37.
- [138] Abe M, Michi T, Sato A, Kondo T, Zhou W, Ye S, et al. *Angew Chem Int Ed* 2003;42:2912–5.
- [139] Altman M, Zenkina OV, Ichiki T, Iron MA, Evmenenko G, Dutta P, et al. *Chem Mater* 2009;21:4676–84.
- [140] Zhao W, Tong B, Pan Y, Shen J, Zhi J, Shi J, et al. *Langmuir* 2009;25:11796–801.
- [141] Zhao W, Tong B, Shi J, Pan Y, Shen J, Zhi J, et al. 2010;26:16084–9.
- [142] Lokesh KS, Chardon-Noblat S, Lafolet F, Traoré Y, Gondran C, Guionneau P, et al. *Langmuir* 2012;28:11779–89.
- [143] Lin C, Kagan CR. *J Am Chem Soc* 2003;125:336–7.
- [144] Kanaizuka K, Murata M, Nishimori Y, Mori I, Nishio K, Masuda H, et al. *Chem Lett* 2005;34:534–5.
- [145] Ohba Y, Kanaizuka K, Murata M, Nishihara H. *Macromol Symp* 2006;235:31–8.
- [146] Nishimori H, Kanaizuka K, Murata M, Nishihara H. *Chem Asian J* 2007;2:367–76.
- [147] Utsuno M, Toshimitsu F, Kume S, Nishihara H. *Macromol Symp* 2008;270:153–60.
- [148] Nishimori Y, Kanaizuka K, Kurita T, Nagatsu T, Segawa Y, Toshimitsu F, et al. *Chem Asian J* 2009;8:1361–7.
- [149] Kurita T, Nishimori Y, Toshimitsu F, Muratsugu S, Kume S, Nishihara H. *J Am Chem Soc* 2010;132:4524–5.
- [150] Nishimori Y, Maeda H, Katagiri S, Sendo J, Miyachi M, Sakamoto R, et al. *Macromol Symp* 2012;317–318:276–85.
- [151] Katagiri S, Sakamoto R, Maeda H, Nishimori Y, Kurita T, Nishihara H. *Chem Eur J* 2013;19:5088–96.
- [152] Maeda H, Sakamoto R, Nishimori Y, Sendo J, Toshimitsu F, Yamanoi Y, et al. *Chem Commun* 2011;47:8644–6.
- [153] Yamanoi Y, Sendo J, Kobayashi T, Maeda H, Yabusaki Y, Miyachi M, et al. *J Am Chem Soc* 2012;134:20433–9.
- [154] Yamanoi Y. *J Org Chem* 2005;70:9607–9.
- [155] Yamanoi Y, Nishihara H. *Tetrahedron Lett* 2006;47:7157–61.
- [156] Yamanoi Y, Taira T, Sato J, Nakamura I, Nishihara H. *Org Lett* 2007;9:4543–6.
- [157] Yamanoi Y, Nishihara H. *J Org Chem* 2008;73:6671–8.
- [158] Yamanoi Y, Nishihara H. *J Synth Org Chem Jpn* 2009;67:778–86.
- [159] Yabusaki Y, Ohshima N, Kondo H, Kusamoto T, Yamanoi Y, Nishihara H. *Chem Eur J* 2010;16:5581–5.
- [160] Lesbani A, Kondo H, Yabusaki Y, Nakai M, Yamanoi Y, Nishihara H. *Chem Eur J* 2010;16:13519–27.
- [161] Kurihara Y, Nishikawa M, Yamanoi Y, Nishihara H. *Chem Commun* 2012;48:11564–6.
- [162] Inubushi H, Kondo H, Lesbani A, Miyachi M, Yamanoi Y, Nishihara H. *Chem Commun* 2013;49:134–6.
- [163] Lesbani A, Kondo H, Sato J-I, Yamanoi Y, Nishihara H. *Chem Commun* 2010;46:7784–6.
- [164] Saraceno RA, Riding GH, Alcock HR, Ewing AG. *J Am Chem Soc* 1988;110:7254–5.
- [165] Petrov EG, Shevchenko YV, Teslenko VI, May V. *J Chem Phys* 2001;115:7107–22.
- [166] Petrov EG, May V. *J Phys Chem A* 2001;105:10176–86.
- [167] Arikuma Y, Nakayama H, Morita T, Kimura S. *Angew Chem Int Ed* 2010;49:1800–4.
- [168] Laviron E. *J Electroanal Chem* 1979;101:19–28.
- [169] Decker F, Cattaruzza F, Coluzza C, Flamini A, Marrani AG, Zanoni R, et al. *J Phys Chem B* 2006;110:7374–9.
- [170] Nagata M, Kondo M, Suemori Y, Ochiai T, Dewa T, Ohtsuka T, et al. *Colloid Surf B* 2008;64:16–21.
- [171] Marrani AG, Dalchiele EA, Zanoni R, Decker F, Cattaruzza F, Bonifazi D, et al. *Acta* 2008;53:3903–9.
- [172] Seo K, Konchenko AV, Lee J, Bang GS, Lee H. *J Mater Chem* 2009;19:7617–24.
- [173] Szymańska I, Stobiecka M, Orlewska C, Rohand T, Janssen D, Dehaen W, et al. *Langmuir* 2008;24:11239–45.
- [174] Foster RJ, Faulkner LR. *J Am Chem Soc* 1994;116:5444–52.
- [175] Chidsey CED. *Science* 1991;251:919–22.
- [176] Sek S, Palys B, Bilewicz R. *J Phys Chem B* 2002;106:5907–14.
- [177] Brooksby PA, Anderson KH, Downard AJ, Abell AD. *Langmuir* 2010;26:1334–9.
- [178] Nahir TM, Bowden EF. *J Electroanal Chem* 1996;410:9–13.
- [179] Abhayawardhana AD, Sutherland TC. *J Phys Chem C* 2009;113:4915–24.
- [180] Arikuma Y, Nakayama H, Morita T, Kimura S. *Langmuir* 2011;27:1530–5.
- [181] Arikuma Y, Takeda K, Morita T, Ohmae M, Kimura S. *J Phys Chem B* 2009;113:6256–66.
- [182] Brooksby PA, Anderson KH, Downard AJ, Abell AD. *J Phys Chem C* 2011;115:7516–26.
- [183] Darwish N, Eggers PK, Ciampi S, Tong Y, Ye S, Paddon-Row MN, et al. *J Am Chem Soc* 2012;134:18401–9.
- [184] Mandal HS, Kraatz H-B. *J Phys Chem Lett* 2012;3:709–13.
- [185] Creager SE, Wooster TT. *Anal Chem* 1998;70:4257–63.
- [186] Li J, Schuler K, Creager SE. *J Electrochem Soc* 2000;147:4584–8.
- [187] Lambert C, Kriegisch V. *Langmuir* 2006;22:8807–12.
- [188] Roth KM, Yasseri AA, Liu Z, Dabke RB, Malinowski V, Schweikart K-H, et al. *J Am Chem Soc* 2003;125:505–17.
- [189] Eckermann AL, Shaw JA, Meade TJ. *Langmuir* 2010;26:2904–13.
- [190] Hong W, Li H, Liu S-X, Fu Y, Li J, Kaliginedi V, et al. *J Am Chem Soc* 2012;134:19425–31.
- [191] Peng Z-L, Chen Z-B, Zhou X-Y, Sun Y-Y, Liang J-H, Niu Z-J, et al. *J Phys Chem C* 2012;116:21699–705.
- [192] Lu Q, Yao C, Wang X, Wang F. *J Phys Chem C* 2012;116:17853–61.
- [193] Li Z, Park T-H, Rawson J, Therien M-J, Borguet E. *Nano Lett* 2012;12:2722–7.
- [194] Wei Z, Li T, Jennum K, Santella M, Bovet N, Hu W, et al. *Langmuir* 2012;28:4016–23.
- [195] Kim B, Choi SH, Zhu X-Y, Frisbie CD. *J Am Chem Soc* 2011;133:19864–77.
- [196] Ishida T, Mizutani Q, Liang T-T, Azebara H, Miyake K, Sasaki S, et al. *Ann NY Acad Sci* 2003;1006:164–86.
- [197] Liu K, Li G, Wang X, Wang F. *J Phys Chem C* 2008;112:4342–9.
- [198] Pourhossein P, Chiechi RC. *ACS Nano* 2012;6:5566–73.
- [199] Wang G, Kim T-W, Lee H, Lee T. *Phys Rev B* 2007;76:205320.
- [200] Yaffe O, Scheres L, Segev L, Biller A, Ron I, Salomon E, et al. *J Phys Chem C* 2010;114:10270–9.
- [201] Tuccitto N, Ferri V, Cavazzini M, Quici S, Zhavnerko G, Licciardello A, et al. *Nat Mater* 2009;8:41–6.
- [202] Kronemeijer AJ, Huisman EH, Akkerman HB, Goossens AM, Katsouras I, van Hal PA, et al. *Appl Phys Lett* 2010;97:173302.
- [203] Neuhausen AB, Hosseini A, Sulpizio JA, Chidsey CED, Goldhaber-Gordon D. *ACS Nano* 2012;6:9920–31.
- [204] Takeda K, Morita T, Kimura S. *J Phys Chem B* 2008;112:12840–50.
- [205] Pawlowski J, Juhaniwicz J, Tymecka D, Sek S. *Langmuir* 2012;28:17287–94.
- [206] Takada T, Kawai K, Fujitsuka M, Majima T. *Chem Eur J* 2005;11:3835–42.
- [207] Kawai K, Matsutani E, Maruyama A, Majima T. *J Am Chem Soc* 2011;133:15568–77.
- [208] Lewis FD, Wu T, Zhang Y, Letsinger RL, Greenfield SR, Wasielewski MR. *Science* 1997;277:673–6.
- [209] Schneebeli ST, Kamenetska M, Cheng Z, Skouta R, Friesner RA, Venkataraman L, et al. *J Am Chem Soc* 2011;133:2136–9.
- [210] Kolivoška V, Valášek M, Gál M, Sokolová R, Bulčíková J, Pospíšil L, et al. *J Phys Chem Lett* 2013;4:589–95.
- [211] Terada K, Nakamura H, Kanaizuka K, Haga M, Asai Y, Ishida T. *ACS Nano* 2012;6:1988–99.
- [212] Carter MT, Rowe GK, Richardson JN, Tender LM, Terrill RH, Murray RW. *J Am Chem Soc* 1995;117:2896–9.
- [213] Sakamoto R, Katagiri S, Maeda H, Nishihara H. *Coord Chem Rev* 2013;257:1493–506.



Hiroaki Maeda was born in Toyama prefecture, Japan in 1987. He graduated from The University of Tokyo in 2010, and received his M. Sc. Degree from the same university in 2012 under the supervision of Prof. Hiroshi Nishihara. He is currently a Ph. D course student in Prof. Nishihara laboratory. His research interests include the stepwise fabrication of nanostructures on electrode based on the coordination chemistry, and their electrochemical evaluation.



Ryota Sakamoto was born in Yamagata Vil., Nagano, Japan in 1980. He graduated from The University of Tokyo (Japan) in 2002, and received his Ph.D. degree from the same university in 2007 under the supervision of Prof. Hiroshi Nishihara. Then he was appointed as an assistant professor at Tokyo University of Science (Japan), working with Prof. Takeshi Yamamura. In 2010 he moved to The University of Tokyo, joining Prof. Nishihara's group again. His current research interest lies on the construction of molecule-based nanostructures, and photonic and electronic devices using thereof.



Hiroshi Nishihara received his B.Sc. degree in 1977, M. Sc. in 1979 and D. Sc. in 1982 from The University of Tokyo. He was appointed research associate of Department of Chemistry, Faculty of Science and Technology at Keio University in 1982, and he was promoted lecturer in 1990, and associate professor in 1992. Since 1996, he has been a professor of Department of Chemistry, School of Science at The University of Tokyo. He also worked as a visiting research associate of Department of Chemistry at The University of North Carolina at Chapel Hill (1987–1989), and as a researcher of PRESTO, JRD (1992–1996). His research has been focused on creation of new electro- and photo-functional materials comprising both transition metals and π -conjugated chains, and invention of unidirectional electron transfer systems utilizing molecular layer interfaces.